

© 2013

Sankha Banerjee

ALL RIGHTS RESERVED

**AN EXPERIMENTAL AND THEORETICAL ANALYSIS OF
TWO AND THREE PHASE EPOXY BASED
PIEZOELECTRIC COMPOSITES**

by

SANKHA BANERJEE

A thesis submitted to the

Graduate School-New Brunswick

Rutgers, The State University of New Jersey

in partial fulfillment of the requirements

for the degree of

Master of Science

Graduate Program in Mechanical and Aerospace Engineering

written under the direction of

Professor Kimberly Cook-Chennault

and approved by

Professor George Weng

Professor Assimina A. Pelegri

and

Professor Kimberly A. Cook-Chennault

New Brunswick, New Jersey

May, 2013

ABSTRACT OF THE THESIS

An experimental and theoretical analysis of two and three phase epoxy based piezoelectric composites

by

SANKHA BANERJEE

Thesis Director:

Professor Kimberly Cook-Chennault

New composite materials and devices have been investigated by researchers in the fields of energy harvesting, structural health monitoring (SHM) of civil and mechanical structures and acoustic attenuation. The criteria that govern the applicability of these types of devices are their sensitivity and durability, which depend on electromechanical properties such as the dielectric constant, piezoelectric strain coefficient, and the dielectric loss. The present work investigates the role of Aluminum and PZT inclusions distributed in an epoxy matrix to fabricate composites with high dielectric and strain coefficients. The influence of Aluminum inclusion size (nano and micron) and (lead zirconate titanate) PZT and Aluminum volume fraction on the electromechanical properties of the three phase PZT-epoxy-aluminum composites were experimentally investigated. An analytical expression for the prediction of the effective dielectric constant of a three phase 0-3-0 piezoelectric composite has also been developed. The analytical results are verified with the experimental results from Nan et al. The analytical model is also extended to include the shape of a conductive inclusion phase; to examine the influence of the shape on the

effective dielectric constant of the composite. The electromechanical properties of the composites are influenced by several factors: inclusion agglomeration, contact resistance between particles, and air voids. The present work studies the influence of these factors on the effective electromechanical properties of the composite.

Acknowledgements

First of all I would like to acknowledge my advisor Prof. Kimberly Cook-Chennault for her continuous support in my research and her meticulous effort in the development of my intellectual ability towards becoming a better researcher and moreover a better person and becoming a valuable member in the society. Her enthusiasm, patience and inspiration has been motivational for me towards improving my intellectual ability and analyzing skills.

Besides my advisor I would like to thank my committee members, Prof. George Weng and Prof. Assimina Peligri for their encouragement, time and helpful insight towards my research work. The members of the Hybrid Energy Systems Laboratory have been an important part of my research and personal life. Without their collaboration and support this thesis would not have been possible.

I would like to thank and show my appreciation to the former and present graduate students, Let Wang, Sean De Gennaro, Udhay Sundar, Andrew Tang, Eric Bickford, and undergraduates Michael and Eric Refour (summer intern). I would also like to thank my friends in Rutgers, Ram C.M. Kalluri, Georgiana Giancola, Alireza Yazdani, Pallab Barai, Hadi Halim for the wonderful times I spend with them, specially the lunch breaks and the long coffee breaks; discussing about naïve and important things about life, research and graduate school and life beyond that.

Lastly I would like to thank my family, specially my parents who have been an inspiration all my life and have motivated me to achieve new heights in my career. I would like to thank and show great appreciation to my lovely and beautiful wife Debaki, who has been with me through all the ups and downs, the happy and sad times through all these years that

we have been together. In spite of being a Biologist she has shown great appreciation and excitement towards my research and has motivated me throughout my professional and academic life to achieve higher standards. Without my parents and my wife's love and emotional support through some of the tough times in my life this thesis would not have been possible.

Sankha Banerjee

Rutgers University

May 2013

Table of Contents

Abstract Of The Thesis	ii
Acknowledgments	iv
Table of Contents	vi
List of Figures.....	viii
List of Tables	xi
Chapter 1. Introduction	1
<i>1.1 .Research motivation.....</i>	<i>1</i>
<i>1.1.1. Piezoelectric materials and electromechanical properties.....</i>	<i>4</i>
<i>1.1.2. Composite piezoelectric materials.....</i>	<i>9</i>
<i>1.2. Literature review of three phase 0-3-0 piezoelectric composites with conductive fillers and challenges to the realization of functional devices and materials</i>	<i>12</i>
<i>1.3. Phenomenon of percolation.....</i>	<i>14</i>
<i>1.4. Overview of the thesis.....</i>	<i>20</i>
 Chapter 2. An analytical model for the prediction of the dielectric constant of three phase 0-3 piezoelectric composites with electrically conductive inclusions	22
<i>2.1. Introduction.....</i>	<i>22</i>
<i>2.2. Methodology.....</i>	<i>26</i>
<i>2.2.1. Three phase analytical model for prediction of the dielectric constant of 0-3-0 composites.....</i>	<i>27</i>
<i>2.2.2. Model Results Discussion: Comparison of model with experimental data.....</i>	<i>31</i>
<i>2.3. Conclusions</i>	<i>34</i>
 Chapter 3. Effect of PZT volume fraction and Al inclusions on three phase 0-3-0 PZT-Epoxy-Al composites	35
<i>3.1. Fabrication of two phase 0-3 PZT-Epoxy composites.....</i>	<i>37</i>
<i>3.2. Fabrication of three phase 0-3-0 PZT-Epoxy-Al micron sized composites</i>	<i>38</i>

3.3. <i>Experimental results and discussions</i>	41
3.4. <i>Three phase PZT-Epoxy-Al composite with varying Al volume fraction</i>	49
3.5. <i>Conclusions</i>	55
 Chapter 4. Effect of PZT volume fraction and the size of Al inclusions on three phase 0-3-0 PZT-Epoxy-Al percolative composites	56
4.1. <i>Fabrication of two phase 0-3 PZT-Epoxy composites</i>	57
4.2. <i>Experimental results and discussions</i>	58
4.3. <i>Conclusions</i>	66
 Chapter 5. Conclusions and future work	68
5.1. <i>Conclusions</i>	68
5.2. <i>Future Work</i>	70
 References	71

List of Figures

FIGURE 1-1 Crystal lattice structures of PZT, A) Perovskite-type lead zirconate titanate (PZT) unit cell in the symmetric cubic state above the Curie temperature, B) Tetragonally distorted unit cell below the Curie temperature where P is the direction of polarization	5
FIGURE 1-2 Aligned dipoles in single crystal piezoelectric materials, B) Dipoles aligned in different local domains in polycrystalline ceramic piezoelectric materials, C) Strong electric field applied along the desired alignment direction	6
FIGURE 1-3 Direction of polarization and forces in a piezoelectric element	8
FIGURE 1-4 Phenomenon of percolation explained by increase in volume fraction of the conductive inclusion in a 2D matrix and the formation of continuous conductive pathways	13
FIGURE 2-1 Representation of uniformly distributed and separated spherical inclusions in a 3 dimensional matrix, a 0-3 composite	21
FIGURE 2-2 Representation of uniformly distributed and separated spherical inclusions in a 3 dimensional matrix, a 0-3 composite	28
FIGURE 2-3 Representation of uniformly distributed and separated spherical inclusions of two different materials in the 3 dimensional matrix, a 0-3-0 composite.....	29
FIGURE 2-4 Spherical and spheroidal inclusions in a 0-3-0 composite	30
FIGURE 2-5 Comparison of the dielectric Constant of the Terfnol D-PZT-PVDF composite [58,111] with Equation (6). The figure also shows that the model has a similar trend to that of the linear best fit of the experimental data	32
FIGURE 2-6 Comparison of the dielectric Constant of the BaTiO ₃ -PVDF-MWNT composite [111,113] with an average MWCNT aspect ratio of 10, with Equation (8).....	33
FIGURE 3-1 Spellman high voltage generator and the high voltage poling fixture used in the contact poling of the two phase 0-3 and three phase 0-3-0 composites.....	38
FIGURE 3-2 Morphologies of the individual phases of the 0-3-0 composite as seen in the SEM micrographs, A) Micron sized Al inclusions, B) PZT particles, and C) Epoxy Matrix.	39
FIGURE 3-3 Experimental procedure for fabrication of three phase 0-3-0 PZT-Epoxy-Al composites	40
FIGURE 3-4 Comparison of the dielectric constant (ϵ) of the two phase 0-3 composite with effective dielectric constant models, namely the Maxwell-Garnett approximation and the Bruggeman's Model, shows the Maxwell-Garnett's model underestimates and the Bruggeman's model overestimates the predicted values of the effective dielectric constant	42
FIGURE 3-5 SEM micrograph of a two phase PZT-Epoxy composite showing the distribution of	

the PZT particles in the Epoxy matrix with PZT volume fraction at 30 %.....	45
FIGURE 3-6 Comparison of the $\tan(\delta)$ of the two phase PZT-Epoxy and three phase PZT-Epoxy-Al composites.....	45
FIGURE 3-7 Comparison of the $\tan(\delta)$ of the two phase PZT-Epoxy and three phase PZT-Epoxy-Al composites.....	46
FIGURE 3-8 Comparison of the piezoelectric strain coefficient, d_{33} of the two phase PZT-Epoxy and three phase PZT-Epoxy-Al composites.....	47
FIGURE 3-9 SEM micrograph of a three phase PZT-Epoxy-Al micro composite showing the distribution of the PZT particles and micron sized Al inclusions in the Epoxy matrix with PZT volume fraction at 50 % and Al volume fraction at 20 %.....	48
FIGURE 3-10 Variation of the piezoelectric strain coefficient, d_{33} and the dielectric loss, $\tan \delta$ as a function of increasing Al volume fraction.....	50
FIGURE 3-11 Variation of the dielectric constant, ϵ of the three phase composite with varying Al volume fraction and comparison with the three phase model.....	50
FIGURE 3-12 Comparison of the $\tan(\delta)$ of the three phase PZT-Epoxy-Aluminum composite with varying Aluminum volume fraction.....	52
FIGURE 3-13 SEM micrograph of a three phase PZT-Epoxy-Al micro composite showing the distribution of the PZT particles and micron sized Al inclusions in the Epoxy matrix with PZT volume fraction at 30 % and Al volume fraction at 17 %.....	52
FIGURE 3-14 Variation of the percolation threshold as demonstrated by the change in d_{33} as a function of varying Al volume fraction, along with the change in PZT volume fraction from 20% to 30%.....	53
FIGURE 3-15 Variation of the as demonstrated by the change in d_{33} as a function of varying Al volume fraction, along with the change in PZT volume fraction from 20% to 30%	54
FIGURE 4-1 SEM micrographs of Al nanoparticles showing A) Clusters of Al nanoparticles and B) Spherical nano-particles.....	58
FIGURE 4-2 A comparison of the dielectric constant of three phase micro and nano composites.....	59
FIGURE 4-3 Comparison of the dielectric loss factor, $\tan \delta$ of the three phase composite with micro and nano sized Al inclusions and with the power law for the loss tangent.....	61
FIGURE 4-4 Comparison of the piezoelectric strain coefficient, d_{33} for the three phase micro and nano composite shows that the d_{33} values for both the set of composites increase after the volume fraction of PZT increases above 30% and that the values of the nano composite are lower than that of the micro composite	61
FIGURE 4-5 SEM micrograph of a three phase PZT-Epoxy-Al nano composite showing the distribution of the PZT particles in the Epoxy matrix with PZT volume fraction at 50 % and Al volume fraction at 20 %.....	62
FIGURE 4-6 SEM micrographs of three phase PZT-Epoxy-Al nano composites at magnifications	

of A) 50,000 X and B) 100,00 X respectively showing the distribution and clusters of the Al nano particles in the Epoxy matrix with PZT volume fraction at 50 % and Al volume fraction at 20 %	63
FIGURE 4-7 Contact points between Al a) nano sized and b) micron sized particles with the surrounding phases and with itself.....	63
FIGURE 4-8 Resistivity of three phase micro and nano PZT-Epoxy-Al composites with varying PZT volume fraction.....	65

List of Tables

Table 1-1	Variation of $\tan \delta$ values in different materials used for dampening applications [8, 13, 37,87,116]	9
Table 1-2	Variation of percolation threshold of two phase composites with different kinds of conductive fillers, filler size and aspect ratios [116]	15
Table 3-1	Physical properties of PZT, EC76.	38

Nomenclature

S	Mechanical Strain
s	Elastic compliance
E	Electric Field
d	Piezoelectric strain coefficient
T	Mechanical Stress
D	Electric charge displacement
ϵ	Dielectric constant (relative permittivity)
ϵ_{Matrix}	Dielectric constant of the 3-dimensional matrix phase in the composite
$\epsilon_{\text{Inclusion}}$	Dielectric constant of the zero-dimensional inclusion in the 3-dimensional matrix
ϵ_{0-3-0}	Dielectric constant of the three phase 0-3-0 composite
ϵ_{PZT}	Dielectric constant of PZT
ϵ_{Epoxy}	Dielectric constant of Epoxy
$\tan \delta$	Tangent of the dielectric loss angle
E'	Elastic storage modulus
E''	Elastic loss modulus
σ	Resistivity
ϕ	Volume fraction of the conductive filler in the composite
ϕ_c	Volume fraction of the conductive filler when the composite reaches the percolation threshold
$\phi_{\text{Inclusion}}$	Volume fraction of the zero-dimensional inclusion in the 3-dimensional matrix
t	Power law constant for the resistivity power law near the percolation threshold
$\phi_{\text{Inclusion}_1}$	Volume fraction of the first zero-dimensional inclusion in the 3-dimensional matrix
$\phi_{\text{Inclusion}_2}$	Volume fraction of the second zero-dimensional inclusion in the 3-dimensional matrix
$B = \frac{1}{3} \sum_{j=a,b,c} A_j^{-1}$	Shape factor of the conductive spheroidal inclusion that depends on the dimensions of the inclusions
$\beta = \epsilon_{\text{PZT}} - \epsilon_{\text{Epoxy}} / \epsilon_{\text{PZT}} + 2 \epsilon_{\text{Epoxy}}$	Coefficient of the Maxwell-Garnett's equation

Chapter 1.

Introduction

1.1. Research motivation

Piezoelectric materials are certain non-conductive materials that generate electric charges when they are subjected to mechanical stress; such as, those caused by vibration and pressure [1-5]. These electric charges are proportional to the amount of the mechanical stress induced in the material. These materials also generate mechanical excitations when they are subjected to an electric field. Piezoelectric materials have no crystalline inversion symmetry and there is a linear interaction between the mechanical and electrical energy of the material [113]. The piezoelectric effect is a reversible process, where there is an internal generation of an electric charge from a mechanical vibration or applied force, and vice versa.

Piezoelectric materials are ubiquitously used in many devices such as sensors [1-10], actuators [11-16], resonators and filters for telecommunication [17-20], transducers for converting electrical energy to mechanical energy, or vice-versa [21-31], embedded passive devices such as capacitors [32-43], and in structural health monitoring applications [43-47]. In addition to the applications mentioned above, piezoelectric materials are employed in electronic frequency generation, sound generation and detection, microbalances, ultrafine focusing in optical instruments, atomic resolution

instruments (e.g. scanning probe microscopes and atomic force microscopes) and other applications that require voltage generation and amplification [1-6, 110, 100, 113, 116].

Piezoelectric materials have received a lot of attention due to their ability to convert mechanical energy directly into electric energy. Thus, in addition to the aforementioned applications of piezoelectric materials, these materials have gained interest because of their possible use as energy harvesting materials, and vibration and sound dampening devices. Specifically, many speculate that these materials can lead to the realization of self-sustainable portable electronic devices and, hybrid battery – piezoelectric device systems [112, 113]. In the case of hybrid energy systems, the coupling of the piezoelectric device with a battery is forecasted to result in the reduction of the mass or size of the overall power supply system. Energy harvesting, or energy scavenging, is the process of deriving energy from ambient waste energy sources, such as vibration, waste heat, solar energy etc, and capturing and storing the energy for use in electronic systems.

Others have also explored the use of these materials for damping of mechanical and structural vibrations and acoustic attenuation [1, 115, 116]. Acoustic liners are presently used for attenuating combustion and turbine noise radiated from jet engines; and have been proposed [81] as a strategy for attenuation of some forms of airframe noise radiated towards the ground. Traditionally, polymers have been the most extensively used; however, these materials must have a high elastic loss modulus or tangent loss factor in order to enhance the distribution of molecular relaxation [81]. In particular, airframe

noise that results from the convection of turbulence through the slat gap and past the trailing edge of the slat, can possibly be attenuated using active composite piezoelectric liners. Specifically, application of voltage excitation to the piezoelectric material results in vibration at a given frequency and displacement, which serves to attenuate noise. Damping materials, such as these; have a good ability to dissipate elastic strain energy when subjected to vibration loads. These materials are ubiquitous in high-performance structural applications, e.g. aerospace, marine, aircraft, construction, automotive, etc. [81]. The acoustic liners that are currently used are passive, and thus only able to absorb acoustic energy over a limited bandwidth [81].

Piezoelectric ceramics face challenges that limit their applications in energy harvesting and acoustic dampening devices. Piezoelectric ceramics exhibit poor mechanical properties and are prone to failure, which limits their applications in acoustic dampening [114]. The brittle nature of piezoelectric ceramics, make these materials susceptible to premature failure when they subjected to static or frequency dependant mechanical loading or mechanical shock [114]. In addition to that; the working range of these materials is restricted over a limited bandwidth. Use of composite piezoelectric materials would address these issues; since the acoustic impedance of these materials could be tuned for optimal attenuation, and also the effective mechanical strength can be improved [110, 111, 116].

Newer polymer based piezoelectric composites are being investigated, whereby the

mechanical vibration energy can be transmitted to a piezoelectric material, and the energy is in-turn converted into electrical potential, via the piezoelectric effect. The electrical potential is then converted into joule heat through networks of electro-conductive particles in the polymeric matrix. This process is referred to as the piezoelectric damping effect [2]. The piezoelectric dampening effect depends on the electromechanical properties of the composite.

The present work focuses on the exploration of two and three phase piezoelectric composites; to understand the effect of the volume fraction of the piezoelectric phase, and the conductive inclusion size, shape and volume fraction, on the electromechanical properties of these materials as a function of the fabrication technique, constituent material properties and micro-structural morphology of the composites.

1.1.1. Piezoelectric materials and electromechanical Properties

On Application of mechanical strain, piezoelectric materials produce an effective electric field [1-5]. Conversely when an electrical field is applied across the material, it results in a mechanical strain or deformation. Many manmade and naturally occurring materials such as quartz, topaz etc. and manmade ceramics such as Barium Titanate (BaTiO_3) [48-51], Lead Titanate and Lead Zirconate Titanate or PZT exhibit piezoelectric properties [52-55]. This effect is due to the formation of crystal lattice structures that have no center of symmetry.

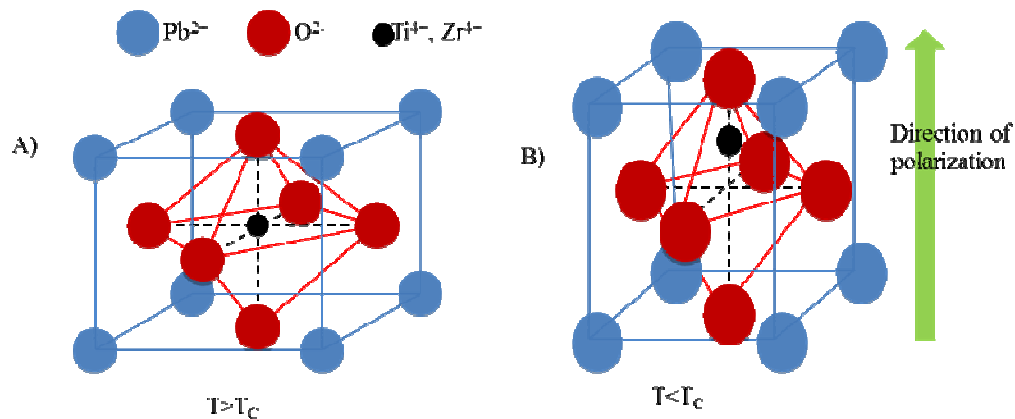


Figure 1-1 Crystal lattice structures of PZT, A) Perovskite-type lead zirconate titanate (PZT) unit cell in the symmetric cubic state above the Curie temperature, B) Tetragonally distorted unit cell below the Curie temperature where the arrow shows the direction of polarization

The asymmetry is caused by the formation of dipoles in the crystal lattice. Each unit cell in a piezoelectric material has a perovskite structure (Figure 1-1). The perovskite structure exists in two crystallographic forms. Below the Curie temperature it takes the form of an asymmetric distorted tetragonal unit cell (Figure 1-1 B), and above the Curie temperature they transform into a cubic structure (Figure 1-1 A). In the tetragonal state, each unit cell has an electric dipole, i.e. there is a small charge differential between each end of the unit cell. This charge differential arises due to the displacement of the central atom (i.e. the Ti or Zr atom in the case of PZT as shown in Figure 1-1) from the center point of the lattice structure. For piezoelectric materials that have a single crystal, the dipoles are aligned in the same direction as shown in Figure 1-2A. In polycrystalline ceramics, such as PZT the dipoles are aligned along certain local domains as can be seen in Figure 1-2B. When a strong electric field is applied across the material, these dipoles can be aligned along a certain direction, as shown in Figure 1-2C. This process of applying a strong electric field is termed as poling.

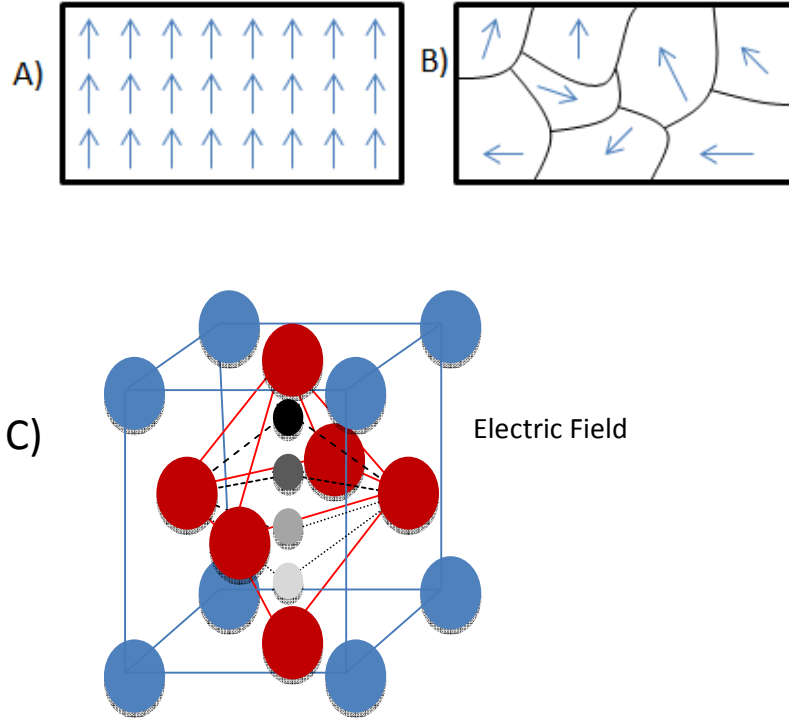


Figure 1-2 A) Aligned dipoles in single crystal piezoelectric materials, B) Dipoles aligned in different local domains in polycrystalline ceramic piezoelectric materials, C) Strong electric field applied along the desired alignment direction

Relationships between applied forces and the resultant responses depend upon the piezoelectric properties of the ceramic, the size and the shape of the material, and the direction of the electrical and mechanical excitation. These relationships can be quantified by the use of electromechanical coefficients. The constitutive equations for a piezoelectric material can be expressed as

$$\{S\} = \left[\left[s^E \right] \{T\} + \left[d^t \right] \{E\} \right] \quad (1.1)$$

$$\{D\} = \left[\left[d \right] \{T\} + \left[\varepsilon^T \right] \{E\} \right] \quad (1.2)$$

where S is the strain, T is the stress, s^E is the elastic compliance at constant electric field, E is the electric field, D is the electric charge displacement, ε^T is the dielectric constant at

a constant stress, and d is the piezoelectric strain constant. Electromechanical coefficients such as; s , d and ϵ , relate both to the direction of the applied mechanical or electrical excitation, and the direction of the response. Each of the coefficients has two subscripts that relate to the directions of the two related quantities. The piezoelectric strain coefficient, d_{ij} ($i = 1, 2, 3, j = 1, 2, \dots, 6$) can be defined as the polarization generated per unit mechanical stress applied to the piezoelectric material or alternatively; the mechanical strain induced per unit electric field applied to the material.

As shown in Figure 1-3 the direction of positive polarization (direction of the effective dipole moment after poling of a piezoelectric material) coincides with the Z axis. The directions X, Y, Z are represented by the numbers 1, 2 and 3 and the shear around these axes is represented by 4, 5, and 6. The first subscript indicates the direction of polarization induced in the material and the second subscript indicates the direction of applied stress or induced strain. It is an important indicator of the efficiency of the material in polarization dependent (energy harvesting) and strain dependent (actuating) applications.

Several properties can be used to examine the performance of piezoelectric materials. One of these is the relative permittivity (dielectric constant) of the material. The relative permittivity or the dielectric constant, ϵ , is the amount of charge that the material can store, relative to the absolute dielectric constant i.e. the charge that can be stored by the same electrodes when separated by a vacuum, at equal voltage (8.85×10^{-12} farad / meter).

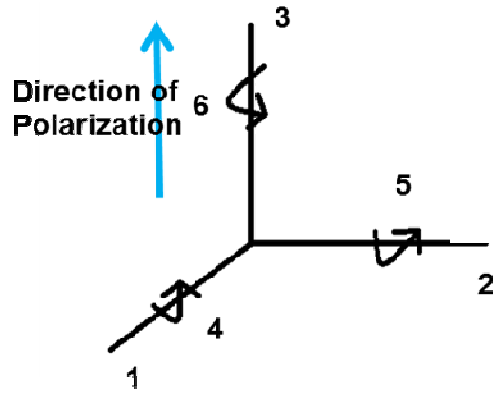


Figure 1-3 Direction of polarization and forces in a piezoelectric element

The electromechanical coupling factor, k_{ij} , is an indicator of the effectiveness with which a piezoelectric material converts electrical energy into mechanical energy, or converts mechanical energy into electrical energy. The first subscript to k denotes the direction along which the electrodes are applied and the second denotes the direction along which the mechanical energy is applied, or developed. The $\tan \delta$, for a ceramic material is the tangent of the dielectric loss angle δ , and is determined by the ratio of effective conductance to effective susceptance in a parallel circuit, measured by using an impedance bridge. $\tan \delta$ is an important parameter in the characterization of the macromolecular viscoelasticity of the material. It represents the damping capacity of the material, and describes the ability of the material to convert mechanical energy into electrical and heat energy, when subjected to an external load. In general, $\tan \delta = E''/E'$, as shown in Equation 1.1, where δ is the phase angle between the stress and strain [81], while E' and E'' are the elastic storage modulus and elastic loss modulus respectively.

$$\tan \delta = \frac{|E| \sin(\delta)}{|E| \cos(\delta)} = \frac{E''}{E'} \quad (1.3)$$

The storage modulus represents the amount of mechanical energy stored during deformation while the loss modulus denotes energy lost as heat during the same deformation cycle. For piezoelectric materials, the dampening capacity is the amount of energy dissipated as heat and electricity one cycle of mechanical vibration. Typical ranges of values for $\tan \delta$ are given in Table 1.1 [8, 13, 37,87,116] for various materials.

Table 1-1 Variation of $\tan \delta$ values in different materials used for dampening applications [8, 13, 37,87,116]

Material	$\tan \delta$
Structural ceramics	10^{-4} to 10^{-5}
Structural metals	0.001 to 0.01
Melamine foams	0.01 to 0.11
Piezoelectric materials	0.01 to 0.9
Natural rubber and viscoelastic polymers	>2

In Composite piezoelectric materials; the electromechanical coefficients, provide a measure of the effect of the individual phases on the effective properties [110,111]. They also relate the effect of the microstructure of the composite material on the effective composite electromechanical characteristics [110, 116].

1.1.2. Composite piezoelectric materials

The electromechanical properties of piezoelectric composites are governed by the arrangement of phases within the composite. The arrangement of phases within the

composite is referred to as connectivity. The concept of connectivity was first developed by Skinner *et al.* [29,56] and later enhanced by Pilgrim *et al.* [57]. In general, 10 connectivity patterns can be used for a diphasic system, which refers to the manner in which individual phases are self-connected. The ten connectivity patterns are (0-0), (0-1), (0-2), (0-3), (1-1), (1-2), (2-2), (1-3), (2-3) and (3-3), where the first digit within the parenthesis refers to the number of dimensions of connectivity for the piezoelectric active phase and the second digit is used for the epoxy phase. This convention can also be extended to include a third phase by adding a third number within the parenthesis [57-60]. Two phase composites have been an active area of research. The addition of a piezoelectric ceramic to a matrix material (which acts as the second phase) retains the mechanical properties of the matrix and shows enhanced electrical properties. These composites exhibit predictable dielectric behavior and low dielectric loss [109, 110, 116, 117,126].

Two-phase composite piezoelectric polymers (CPPs), so-called 0-3 composites comprised of piezoelectric particles embedded within a continuous matrix, have attracted much attention due to their flexibility, ease of processing and use in embedded passive devices [32-43], such as capacitors. Integration of embedded passive components into printed circuit boards generally results in enhanced electrical performance of the device, improved reliability, reduction of device size, faster switching speed, and lower production costs [34, 35, 40]. Two-phase composites: metal-polymer and ceramic-polymer have been extensively studied [32,43,44,56,59,61-68] for application to coupling or by-pass capacitor technology, wherein emphasis has been placed on

achievement of high effective dielectric constants via analysis based on percolation theory and mixing rules. Analytical modeling for predicting the effective dielectric constant of two phase 0-3 composites has been very useful in analyzing the dielectric characteristics of the composites [69-71]. Analytical expressions also act as very important tools in establishing the validity of the experiments conducted on these composites.

The challenges associated with this type of 0-3 connectivity composite are that: 1) it is difficult to achieve uniform distribution of ceramic particles within the polymer matrix, especially at high volume fractions of the ceramic powder, and 2) voids within the composite lead to dielectric breakdown and ultimately poor poling. To reduce problems associated with this type of composite, colloidal processing [76] has been adopted by many, wherein the ceramic powder is coated with a polymer. Polymer-powder coacervates are then precipitated out when a non-solvent is added to the mixture. The coacervates are then filtrated and die pressed. Though this process alleviates many of the issues associated with uniform distribution of particles, difficulty in poling for 0-3 connectivity composites remains a problem. Specifically, in a 0-3 composite the electric field that acts on an individual spherical piezoelectric grain is controlled primarily by the dielectric constant of the polymer phase. Since most polymers have lower dielectric constants compared to ceramic piezoelectric materials, the applied electric field lines usually condense in the lower dielectric constant phase. This issue is addressed by enhancing the conductivity of the polymer phase by adding a conductive material.

1.2. Literature review of three phase 0-3-0 piezoelectric composites with conductive fillers and challenges to the realization of functional devices and materials

Inclusion of conductive fillers within polymer matrices has been demonstrated by several other workers [38,63,77,79,80]. All have reported that the polymer matrix conductivity was enhanced by the electrically conductive filler. Ma and Wang [65] compared the microstructure and dielectric properties of epoxy-based damping composites that contained carbon nanotubes (CNTs) and PMN PZT piezoceramics. They observed that; with the increase in the volume fraction of the conductive inclusion in a two or a three phase, 0-3 or a 0-3-0 composite, the conductivity of the composite increases. This increase is due to the formation of conductive pathways in the matrix as shown in Figure 1-4, which is called percolation. They concluded that the composites exhibited a percolation threshold in the range of 1.0–1.5 g CNTs per 100 g epoxy. They also concluded that in the region of the percolation threshold, a continuous electro-conductive network was formed, and that beyond the percolation threshold, these materials demonstrated dynamic mechanical loss factors that were superior to those below the percolation threshold, and those without semiconductive inclusions. Tian and Wang [66] also examined the performance of epoxy-multiwalled carbon nanotube-piezoelectric ceramic composites as rigid damping materials. Their results were similar to Ma and Wang [65], where the percolation threshold was found to be in the range of 1.0–1.5 g CNTs per 100 g epoxy. They too concluded that loss factors were improved with the incorporation of CNT and (PZT), where the amount of CNT was above

the critical electrical percolation loading.

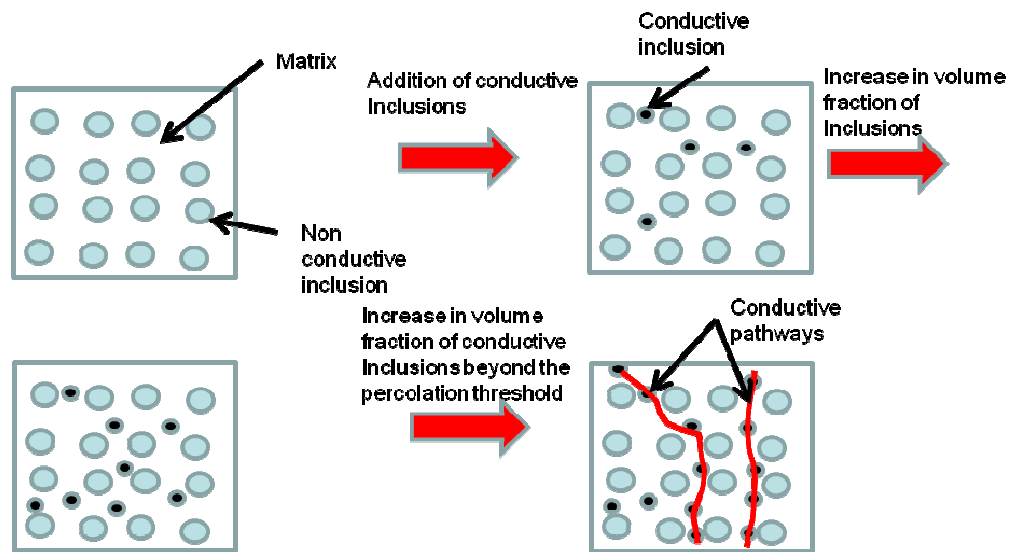


Figure 1-4 Phenomenon of percolation explained by increase in volume fraction of the conductive inclusion in a 2D matrix and the formation of continuous conductive pathways

Hori et al. [78] found that three phase composites produced superior damping loss values in comparison to two-phase composites for specific volume fractions of piezoelectric and conductive material. They fabricated samples that comprised of PZT, carbon black and epoxy. The three phase composite achieved a maximum value of damping loss ~ 0.08 for 0.51 wt.% of carbon black, which corresponded to PZT/CB/EP (69.7/0.5/29.8). This value of damping loss was a substantial increase from the single phase -100% epoxy and two phase, PZT-epoxy composites (70/30 in wt. %) that had loss factors of 0.035 and 0.05, respectively. They found that when the carbon black content was ≤ 0.45 wt. %, the blends behaved electrically as insulators, wherein the electric energy generated from PZT was not fully dissipated. However, for carbon black content ranges from 0.45 to 0.51 wt. %, the generated electric current flowed in the blends through carbon black particles, which resulted in enhanced damping loss values.

The size of the piezoelectric particles within the composite also has an influence on the dielectric constant of the three phase composites. The dielectric constant of the three phase CPP [38,39,80], BaTiO₃–PMMA–Ni comprised of micron size BaTiO₃ particles was found to be ~ 150 in comparison to 100 for three phase composites with nanosize BaTiO₃ particles. The effects of the piezoelectric particle size on the bulk properties of the composite were attributed to the increase in percolation threshold of nickel that was caused when individual or aggregate BaTiO₃ particles surrounded the nickel particles [79]. Percolation of the composite is an important phenomenon that governs the electromechanical characteristics of the composite. Optimal electromechanical properties of the composite can be achieved by tailoring the percolation threshold and the percolation region [38, 39, 79]. In this work the role of percolation along with the determination of the percolation threshold and the effect of the volume fraction of the inclusions has been studied. The next section describes the percolation phenomenon, and presents a literature review of the effect of percolation on the dielectric and piezoelectric properties of two and three phase composites.

1.3. Phenomenon of Percolation

The critical volume fraction of conducting filler in an insulating matrix, above which the electrical or thermal conductivity increases dramatically due to the development of a continuous path of electron transport, so called, percolation threshold, is a function of the conductive inclusion geometry, dispersion within the matrix material, type of insulating matrix, and type of connectivity between particles (e.g. tunneling versus Schottky barrier)

[81, 82]. According to the classical percolation theory, which assumes a physical connection between particles, resistivity or conductivity near the percolation threshold is described by [82]

$$\sigma \propto (\phi - \phi_c)^t \quad (1.5)$$

where ϕ is the volume fraction of the filler, ϕ_c is the percolation threshold, and t is a power law constant that depends on the geometry of the system.

Theoretical values for the range of critical threshold of two phase composites, ϕ_c and t are approximately 0.16-0.17 and 2, respectively for micron sized spherical particles [82, 83]. Many researchers have experimentally demonstrated percolation of spherical and spheroid micron sized conductive particles to be within the range of 0.16 to 0.30 [55, 56] for two phase composites. Also, researchers have shown that for filler particles with high aspect ratios, i.e. shapes that are far from spherical, percolation can occur well below the theoretical value of 0.16 [81, 56-60, 76]. Some examples of two phase conductive composites along with their corresponding percolation thresholds are presented in Table 1-2.

Table 1-2. Variation of percolation threshold of two phase composites with different kinds of conductive fillers, filler size and aspect ratios [116]

Conductive Filler	Fabrication Method	Percolation (volume %)
Graphite flakes, average, 500 μm [7]	Two-roll mill	4.46
Graphite flakes, 50-1000 μm [27]	In situ polymerization	0.878
Graphite flakes, 10-20 μm [8]	Solution blending	0.529
graphite flakes [5]	Solution blending	0.67
Table 1-2. Continued from page 15		

Graphite flakes [6]	Sonication and shear mixing	0.5
Nonentangled MWNT, mean diameter = 50nm, length = 43 ± 3 μ m [24]	Shear mixing	0.0021 -0.0039
Entangled MWNT [17], mean diameter = 120 nm	Magnetic agitation	0.4 - 1.2
Nanostructured metal (Pd,Sn, Cu), 7 - 10 nm, [16]	Vacuum co-condensation	10.0-12.0
Copper nanoparticles, 20 nm, 50 nm, 100 nm Silver nanoparticles, 20 nm, [12]	Ultrasonication	5.0, 5.0, 5.0 5.0
Silver nanoparticles, diameter = 60 nm, length-polymer to silver size ratio:4.2, 7.5 and 23.3 [3]	Two-step mixing	9.3, 7.8
Silver nanoparticles, diameter = 0.4-1 μ m, polymer to silver size ratio: 1.4-3.5 [3]	Two-step mixing	9.1
Silver nanoparticles, diameter = 1.3-3.2 μ m, polymer to silver size ratio: 0.4-1.1 [3]	Two step mixing	19.0
Silver nano sized particles, 100 nm (slightly agglomerated particles) [4]	Batch mixing process in the melt state	13-16
Silver nano sized particles, 100 nm (heavily agglomerated particles) [4]	Batch mixing process in the melt state	20

Application of expression for conductivity in Equation 1.5 becomes more complicated when the composite is comprised of conductive inclusions that are nano in scale. First, use of nanofillers in composites can result in a thin polymer layer encasement of the nanoparticle, which prevents particle to particle contact, resulting in percolation not via particle-to-particle contact, but via tunneling conduction through the interstitial layer [82]. Hence, (for well distributed particles) as the particle size decreases the interparticle spacing decreases and, smaller particles can reach an interparticle distance equal to the tunneling distance at lower percolation thresholds [81]. Many researchers have investigated the percolation threshold of nanocomposites, and have demonstrated

percolation thresholds that range from 0.0021 to 0.19 depending on the filler loading, particle shape, size, processing technique, distribution within the matrix, and aspect ratio of the nanoparticle and epoxy hardener used [82, 83-89]. Some examples of such work are found in Table 1, and a more extensive review of nanotube composites and their percolation behavior may be found in [59, 82, 37,90, 98].

On the other hand, for composites where agglomeration of particles is prevalent, the agglomerations are not necessarily spherical, and can exhibit aspect ratios greater than 1 and can fill a larger volume of fractal shape. Hence, agglomerations can result in localized percolation regions. Increases in nano-filler clustering can result in the loss of inter-phase volume and obstruction of the formation of a percolating inter-phase network in the nano-composite [87, 89]. Particle agglomeration and phase separation over large length scales is detrimental to the electrical properties of the composite [85, 86]. For example, Chan et al. [85] concluded that incorporation of metal nanoparticles does not promise better electrical properties because agglomeration and sedimentation of nano particles detrimentally influences the electrical conductivity. Karttunen [57] found that when nano sized silver particles embedded within a thermoplastic elastomer were slightly agglomerated, the percolation threshold was 13-16%, and the resistance was $2.0 \times 10^{-1} \Omega\text{-cm}$. However, for heavily agglomerated particles, the percolation was 20% with higher resistivity equal to $2.9 \times 10^3 \Omega\text{-cm}$. Tchoudakov et al. [124] studied conductive composites comprised of silver particles dispersed in a liquid epoxy resin, and examined the influence of adding a third component to the mixture carbon black (CB) or carbon fibrils (CF). In the epoxy-silver-CB composites, large Ag agglomerates were observed

and CB networks were not clearly visible. They concluded that this was due to the mutual disturbance of the two conductive networks, wherein the CB hindered the distribution of the Ag particles in the resin. They also stated that the presence of the Ag particles disturbed the connectivity of the CB network. This disturbance of conductive networks was not evidenced in the epoxy-silver-CF composites. Instead, the carbon fibrils were seen to act as conducting bridges, by interconnecting the dispersed Ag agglomerates, which resulted in better conductivity of the composite.

Inclusion of conductive fillers within the polymer matrix of a piezoelectric composite has been demonstrated by several workers [65, 67, 78], wherein the polymer matrix conductivity is enhanced via the electrically conductive filler. The expression for conductivity in Equation 1.5 in theory is used to describe behavior of two phase composites. When the composite is comprised of more than two phases, the percolation behavior can deviate from the predictions of this. However, just as in two phase composites, the size and distribution of particles in the matrix plays a critical role. Choi et al. [100] explored the effects of ferroelectric BaTiO₃ particles on the dielectric behavior of BaTiO₃-Ni-polymethyl methacrylate composites that were fabricated by a two-step mixing and hot-molding method. They concluded that the concentration and particle size of BaTiO₃ influences the composite's dielectric constant, dielectric loss and percolation threshold. Specifically, as the particle size of BaTiO₃ decreased from 1 μm to 80 nm, the percolation threshold of Ni increased. Hence, the percolation threshold of Ni increased respectively, from 8.5 to 10 for 10 vol% of BaTiO₃ and from 13.5 to 15.5 for 20% of BaTiO₃ in BaTiO₃-Ni-PMMA composites when smaller particles of BaTiO₃, an

average size of 80 nm were used instead of 1 μm BaTiO₃ [100]. They concluded that the dielectric properties of the composites comprised of micron sized BaTiO₃ exhibited higher dielectric constant values than those comprised of nano sized BaTiO₃. Wang et al. [38] prepared composites comprised of polymerized styrene-butadiene rubber (SSBR) filled with SiO₂ and carbon black (CB) by reaction blending. They found that due to the nano-dispersion of SiO₂ and CB in the SSBR/SiO₂/CB composites, the conductivity of the composite would decrease if the CB particles were separated by SiO₂ for a certain distance. They claimed that this behavior was based on tunneling conductivity theory, wherein as the isolation distance between the CB particles was less than 10 nm (or shortened to 10 nm via external forces), the electron transition would occur. These composites exhibited the percolation threshold when the ratio of SiO₂/CB was 35/35 and SSBR filler was 70 phr. Ma et al. [65] compared the microstructure and properties of epoxy-based composites containing carbon nanotubes, and PMN-PZT piezoceramics for rigid damping materials. They found that the composites exhibited a percolation threshold in the range of 1.0-1.5 g CNTs per 100g epoxy. They also concluded that in the region of the percolation threshold, a continuous electro-conductive network was formed, and that beyond the percolation threshold, these materials demonstrated dynamic mechanical loss factors that were superior to those below the percolation threshold, and those without semi-conductive inclusions. Tian et al. [66] also fabricated and examined the performance of epoxy/multi-walled carbon nano-tube/piezoelectric ceramic composites as rigid damping materials. Their results were similar to Ma et al.'s, wherein the percolation threshold was found to be in the range of 1.0-1.5 g CNTs per 100g epoxy.

They too, concluded that loss factors were improved with the incorporation of CNT and PZT, where the amount of CNT was above the critical electrical percolation loading.

Many researchers have examined the influence of the aspect ratio of piezoelectric fillers on performance parameters, such as dielectric loss, strain coefficients, and capacitance, but little has been investigated by way of the influence of conductive filler size on three phase piezoelectric composites. In this work, Aluminum micro and nano sized particles are explored as conductive inclusions because they are good electrical conductors, 61% IACS, have a low density, 2.6 gm/cm³, are relatively low cost and are chemically inert in nature. The purpose of this study was to determine if conductive inclusion size, influences the dielectric constant, ϵ , strain coefficient, d_{33} , and loss factor, $\tan(\delta)$ in these types of composites.

1.4. Overview of the Thesis

The present thesis is organized in the following manner; Chapter 2 deals with the development and validation of an analytical model, for predicting the effective dielectric constant of a three phase 0-3-0 composite with spherical and spheroidal inclusions; in Chapter 3 the fabrication of two and three phase 0-3-0, PZT-Epoxy-Al composites with varying PZT and Aluminum volume fraction has been demonstrated and the effect of the varying volume fraction, and the micro-structural properties on the electromechanical characteristics and the percolation threshold has been discussed; Chapter 4 deals with the effect of varying conductive inclusion (Aluminum) size on the dielectric and piezoelectric properties of the three phase composites. Finally in Chapter 5 the conclusion

of the thesis is presented.

Chapter 2.

An analytical model for the prediction of the dielectric constant of three phase 0-3 piezoelectric composites with electrically conductive inclusions

An analytical expression for prediction of the effective dielectric constant of a three phase 0-3-0 ferroelectric composite is presented. The analytical results are verified with the experimental results from Nan et al. [59]. The analytical model is extended to include the shape of a third phase inclusion to examine the influence of the shape (of the inclusion) on the effective dielectric constant of the composite. These analytical results are compared with that of the three phase BaTiO₃-PVDF-MWNT composites from Yao et al. [77] where the average aspect ratio of the conductive MWNT is about 10. A comparison of the analytical predictions with the experimental values indicates that the increase in aspect ratio of the inclusions has a significant effect on the overall dielectric constant of the composite.

2.1 Introduction

Composite ferroelectric materials have been investigated for smart materials in applications such as structural health monitoring of civil structures [44- 46, 59] magnetoelectric sensors [59], and transducer applications [103]. Toward the development of structural health monitoring sensors, researchers have developed cement based 0-3

piezoelectric composites [44-46] because of their compatibility with materials commonly used for civil structural applications; tunable acoustic impedance that can be matched to the host structural material and piezoelectric strain coefficients that are higher than polymer based composites, e.g., 30 (pC/N) and 9 (pC/N) for piezoelectric-cement and polymer based composites, respectively, with equal volume fractions of the piezoelectric transducer (PZT). Also, 0-3 PZT-cement composites can have higher electromechanical coupling factors (20% and 15% for a PZT-cement and polymer based composites, respectively), for smaller volume fractions of PZT, e.g., 0.7 and 0.8 for PZT-cement and polymer based composites, respectively [44-46, 47, 102, 103].

In order to enhance the dielectric constant and electromechanical properties of 0-3 composites, researchers have begun to investigate three phase, 0-3-0 composites. For example, percolative three phase composites comprised of uniformly distributed conductive filler particles within a ferroelectric polymer matrix have been studied [38, 59, 63, 79, 104]; because these materials demonstrate an increase in dielectric properties with an increase in the conductive filler content. Researchers have also concluded that the dielectric constant and piezoelectric strain coefficient of these materials are highly sensitive to the conductive phase content above the percolation limit and within the percolation transition. They have also concluded that having a conductive phase with content above the percolation limit can result in substantial dielectric loss and leakage current. Hence, these researchers have concluded that three phase materials such as these are practical for application below the percolation limit [77, 105, 106]. Here, we present

an analytical model for the prediction of the effective dielectric constant of a three phase piezoelectric composite material, that is, comprised of piezoelectric, matrix and conductive materials that possess 0-3-0 connectivity. We then use this model to investigate the influence of conductive inclusion shape on the effective dielectric constant of the composite.

For this work, the first and third phases are piezoelectric and conductive materials that are distributed within the host matrix, while the second phase is matrix material that is self-connected in three dimensions. Analytical expressions for the effective dielectric constant of a 0-3 composite have been developed by many researchers [61, 69-76]. The model developed by Jayasundere and Smith [73] requires the dielectric constant of the piezoelectric inclusion be greater than that of the host matrix. Thus, this formula is not valid; when the dielectric constant of the inclusion is less than that of the host matrix. On the other hand, Bruggeman's model [70] is valid for inclusions having any dielectric constant but is limited due to its nonlinear and implicit nature. Poon and Shin [72] developed a simple explicit formula for the estimation the effective dielectric constant of a 0-3 composite, wherein the inclusions must be uniformly distributed and separated from each other. In this model, it was assumed the electric displacement of a single particle was due to the effect of both the matrix and the polarization of the inclusions distributed uniformly inside the matrix. For 0-3 composites the effective dielectric constant as predicted by the Maxwell-Garnett, Bruggeman and the Poon and Shin's models can be expressed in terms of the individual dielectric constants of the matrix and the

piezoelectric inclusions as

$$\varepsilon = \varepsilon_{Matrix} \left[1 + \frac{1 + 3\phi_{Inclusion} \beta}{1 - \phi_{Inclusion} \beta} \right] \quad (2.1)$$

$$\varepsilon = (1 - \phi_{Inclusion}) \frac{\varepsilon_{Matrix} - \varepsilon}{\varepsilon_{Matrix} + 2\varepsilon} + \phi_{Inclusion} \frac{\varepsilon_{Inclusion} - \varepsilon}{\varepsilon_{Inclusion} + 2\varepsilon} \quad (2.2)$$

$$\varepsilon = \varepsilon_{Matrix} + \phi_{Inclusion} (\varepsilon_{Inclusion} - \varepsilon_{Matrix}) \times \left[\frac{1}{\phi_{Inclusion} + \frac{1}{3}(1 - \phi_{Inclusion}) \left[\frac{\varepsilon_{Inclusion}}{\varepsilon_{Matrix}} (1 - \phi_{Inclusion}) + \phi_{Inclusion} + 2 \right]} \right] \quad (2.3)$$

where $\phi_{Inclusion}$ is the volume fraction of piezoelectric inclusion, $\beta = (\varepsilon_{Inclusion} - \varepsilon_{Matrix}) / (\varepsilon_{Inclusion} + 2\varepsilon_{Matrix})$ and ε is the dielectric constant of the 0-3 composite.

Researchers such as Han *et al.* [76] have investigated the influence of the polymer on the resistivity and dielectric properties of 0-3 composites. Han *et al.* [76] compared lead titanate (PT) composites with Ecogel polymer, PVDF copolymer and ethylene-propylene-diene monomer (EPDM) polymer. They found that the higher electrical conductivity polymer matrix created more electric flux paths between the ceramic particles, which increased the electric field acting on the ceramic particles, and ultimately made the poling of the ceramic easier, e.g. possible at lower voltage values.

Here, we derive an analytical expression for the prediction of the effective dielectric constant of a three phase 0-3-0 ferroelectric composite, which has not to our knowledge been done before [109,125]. In our model, we assume the first and third phase inclusions

are uniformly distributed and separated from each other. The results for the analytical model are then compared with the experimental results from Nan et al. [59]. The shape of a dispersed particle plays a very important role in the effective dielectric constant of a conductor-dielectric composite [68, 107]; and the deviation of the conductive particle from the spherical form results in higher dielectric constants of the composite [68, 107, 108]. Thus, we extend our analytical model to include the shape of the third phase inclusion to examine the influence of the shape (of the inclusion) on the effective dielectric constant of the composite. These results are then compared with the analytical results for spherical and spheroidal particles.

2.2 Methodology

Let us consider a single spherical inclusion with dielectric constant $\epsilon_{\text{Inclusion}}$ inside an infinite matrix of dielectric constant ϵ_{Matrix} , as depicted in Figure 2-1. In a two phase 0-3 composite, the inclusions are considered to be uniformly distributed and dispersed within the matrix, which is considered to be a continuum medium. This 0-3 composite can be considered as an isotropic material [64,109]. The 0-3-0 material we investigate here is shown in Fig. 2-2, wherein the third phase of 0-3-0 composite is assumed to be spherical conductive inclusions uniformly distributed and separated in the continuum of the isotropic 0-3 composite matrix.

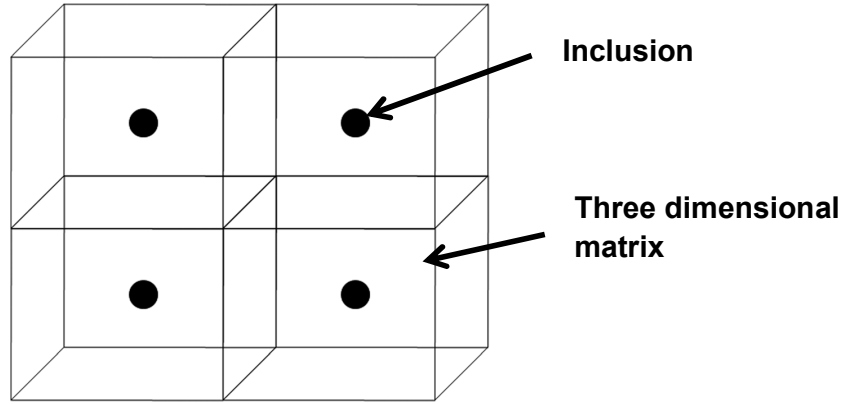


Figure 2-1 Representation of uniformly distributed and separated spherical inclusions in a 3 dimensional matrix, a 0-3 composite

2.2.1 Three phase analytical model for prediction of the dielectric constant of 0-3-0 composites

We first consider a 0-3 composite material when an external field is applied across the z-axis. Here, the electric field inside the matrix and that inside the inclusion are assumed to be uniform and parallel to each other.

The displacement field experienced by a single particle is considered as a sum of two parts; the first part due to the infinite matrix and the other due to the polarization of all the inclusions embedded inside the infinite matrix. The effective dielectric constant ϵ , of a 0-3 composite can be expressed by equation (2.3) as [72]

$$\epsilon = \epsilon_{Matrix} + \phi_{Inclusion_1} (\epsilon_{Inclusion_1} - \epsilon_{Matrix}) \times \left(\frac{1}{\phi_{Inclusion_1} + \frac{1}{3} (1 - \phi_{Inclusion_1}) \left[\frac{\epsilon_{Inclusion_1}}{\epsilon_{Matrix}} (1 - \phi_{Inclusion_1}) + \phi_{Inclusion_1} + 2 \right]} \right) \quad (2.4)$$

where Inclusion_1 refers to the first inclusion in the matrix.

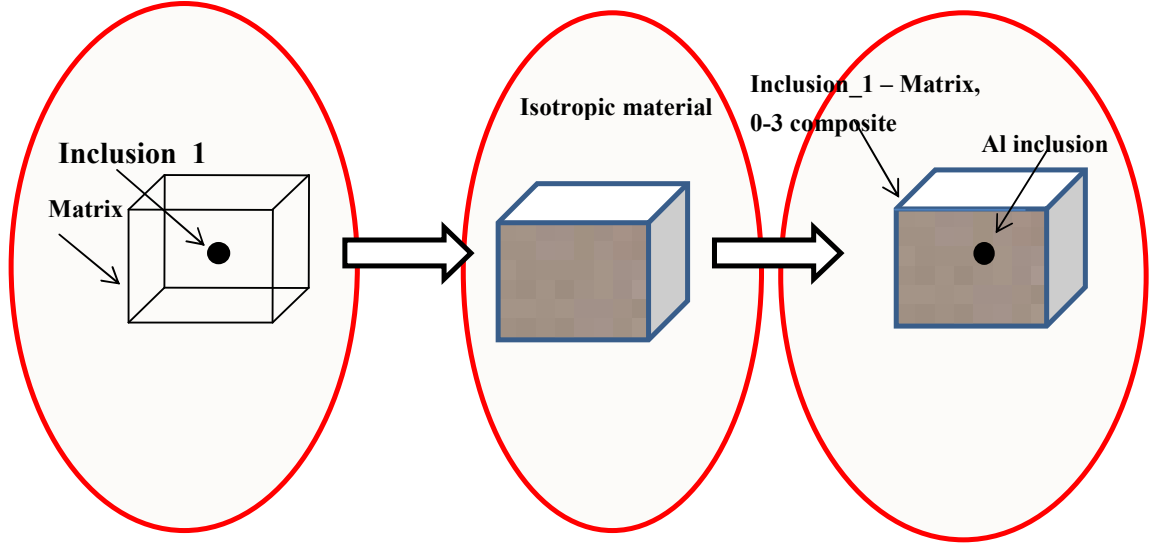


Figure 2-2 Representation of uniformly distributed and separated spherical inclusions in a 3 dimensional matrix, a 0-3 composite

We can extend the expression provided in Equation (2.4) for a 0-3 composite, by the assumption that the 0-3 composite is an isotropic material and including a second inclusion or a third phase, and thus define the effective dielectric constant of the 0-3-0 composite as [109,125]

$$\epsilon_{0-3-0} = \left(\frac{\epsilon_{Matrix} + \phi_{Inclusion_1}(\epsilon_{Inclusion_1} - \epsilon_{Matrix}) \times 1}{\phi_{Inclusion_1} + \frac{1}{3}(1 - \phi_{Inclusion_1}) \left[\frac{\epsilon_{Inclusion_1}}{\epsilon_{Matrix}} (1 - \phi_{Inclusion_1}) + \phi_{Inclusion_1} + 2 \right]} \right) \times \left[\frac{\epsilon_{Inclusion_2} - \epsilon_{Matrix}(\epsilon_{Inclusion_1} - \epsilon_{Matrix}) \times 1}{\phi_{Inclusion_1} + \frac{1}{3}(1 - \phi_{Inclusion_1}) \left[\frac{\epsilon_{Inclusion_1}}{\epsilon_{Matrix}} (1 - \phi_{Inclusion_1}) + \phi_{Inclusion_1} + 2 \right]} \right] + \phi_{Inclusion_2} \left[\frac{1}{\phi_{Inclusion_2} + \frac{1}{3}(1 - \phi_{Inclusion_2}) \left[\frac{\epsilon_{Inclusion_2}}{\epsilon} (1 - \phi_{Inclusion_2}) + \phi_{Inclusion_2} + 2 \right]} \right]$$

(2.5)

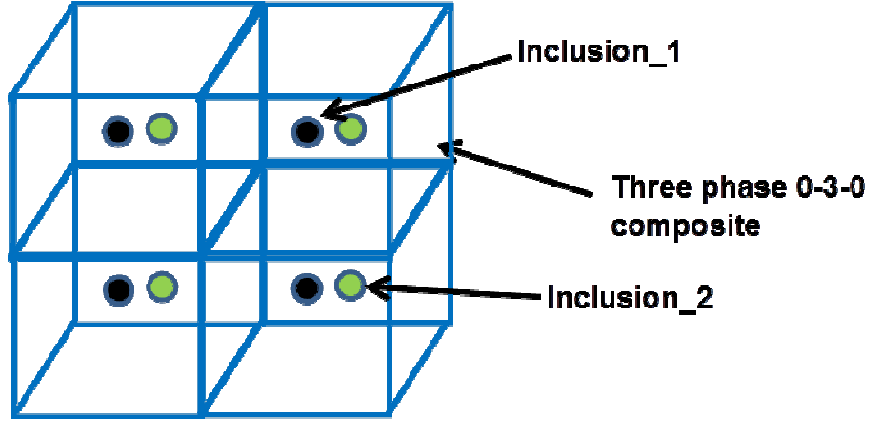


Figure 2-3 Representation of uniformly distributed and separated spherical inclusions of two different materials in the 3 dimensional matrix, a 0-3-0 composite

If the second inclusion of the 0-3-0 composite is a conductive material, its dielectric constant, is infinite [108,109]. Hence, Equation (2.5) reduces to

$$\begin{aligned} \epsilon_{0-3-0} = & \left(\left(\epsilon_{Matrix} + \phi_{Inclusion_1} (\epsilon_{Inclusion_1} - \epsilon_{Matrix}) \times \right. \right. \\ & \left. \left. \frac{1}{\phi_{Inclusion_1} + \frac{1}{3} (1 - \phi_{Inclusion_1}) \left[\frac{\epsilon_{Inclusion_1}}{\epsilon_{Matrix}} (1 - \phi_{Inclusion_1}) + \phi_{Inclusion_1} + 2 \right]} \right) \right) \\ & + \phi_{Inclusion_2} \times \\ & \frac{3 \times \left(\left(\epsilon_{Matrix} + \phi_{Inclusion_1} (\epsilon_{Inclusion_1} - \epsilon_{Matrix}) \times \right. \right. \\ & \left. \left. \frac{1}{\phi_{Inclusion_1} + \frac{1}{3} (1 - \phi_{Inclusion_1}) \left[\frac{\epsilon_{Inclusion_1}}{\epsilon_{Matrix}} (1 - \phi_{Inclusion_1}) + \phi_{Inclusion_1} + 2 \right]} \right) \right)}{(1 - \phi_{Inclusion_2})^2} \end{aligned} \quad (2.6)$$

Since the shape of the conductive filler particle influences the effective dielectric constant of the 0-3-0 composite [59,109], we include a shape factor to take into consideration the shape and the aspect ratio of the inclusions. If we consider the case where the first and second phases in the composite are spheroidal conductive inclusions as shown in Figure 2-4 (aspect ratio >1), and the matrix; the effective dielectric constant of the 0-3 composite can be expressed as [108,109]

$$\varepsilon_{0-3} = \varepsilon_{Matrix} (1 - \phi_{Inclusion_2})^{-B} \quad (2.7)$$

where $B = \frac{1}{3} \sum_{j=a,b,c} A_j^{-1}$ and $A_j = \frac{abc}{3} \int_0^\infty \frac{dt}{[(t+j^2)(t+a^2)(t+b^2)(t+c^2)]^{\frac{1}{2}}}$; a, b and c are

shown in Figure 2-4.

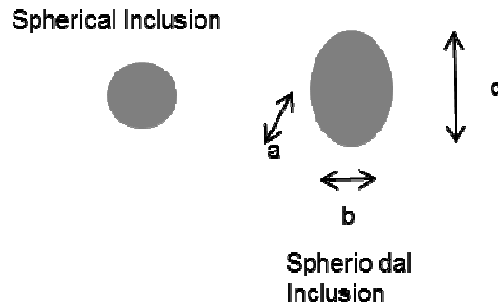


Figure 2-4 Spherical and spheroidal inclusions in a 0-3-0 composite

Assuming that the third phase in the 0-3-0 composite is a spherical conductive inclusion (spheroidal inclusion with aspect ratio ≥ 1), then the dielectric constant of the three phase composite can be given by Equation (2.4) and Equation (2.7) and it takes the form [109]

$$\varepsilon_{0-3-0} = \varepsilon_{Matrix} \left(\frac{1 + \phi_{Inclusion_1} \left(\frac{\varepsilon_{Inclusion_1}}{\varepsilon_{Matrix}} - 1 \right)}{\phi_{Inclusion_1} + \frac{1}{3}(1 - \phi_1) \left[\frac{\varepsilon_{Inclusion_1}}{\varepsilon_{Matrix}} (1 - \phi_{Inclusion_1}) + \phi_{Inclusion_1} + 2 \right]} \right) \times (1 - \phi_{Inclusion_2})^{-B} \quad (2.8)$$

For an increase in aspect ratio for the spheroidal inclusion the dielectric properties of the 0-3-0 composite is enhanced [108,109,111]. Therefore, a deviation of the conductive inclusion size from spherical particles with aspect ratio = 1, to higher aspect ratios, will increase the dielectric constant for the same volume fraction of the inclusion.

2.2.2 Model results and discussion: Comparison of model with experimental data

The analytical expression for the effective dielectric constant of 0-3-0 composites with conductive inclusions were determined using Equation (2.6) and Equation (2.8) and compared with experimental data from Nan et al. [59,109], as shown in Fig. 3. Here, the three phase 0-3-0 composite under consideration is PZT - PVDF - (Terfenol-D), where Terfenol-D is the conducting phase and thus, the third phase for our model. Both the PZT and Terfenol-D inclusions are of micron size.

The effective dielectric constant calculated from Equation (2.6), the experimental data and the data from the linear best fit to the experimental data are presented in Figure 2-5. The predicted values for effective dielectric constant compare well with the experimental

data up to a volume fraction of 0.7 of the conducting phase of Terfenol-D, after which the composite reaches the percolation transition region. When the composite is in the percolation transition region and volume fraction of the conductive inclusion goes above the percolation limit; the composite ceases to be a 0-3-0 composite due to the formation of several linear percolation paths. Our model does not take the percolation transition into consideration. Thus, this model is valid in the region where the volume fraction of the conductive inclusion does not reach the percolation transition.

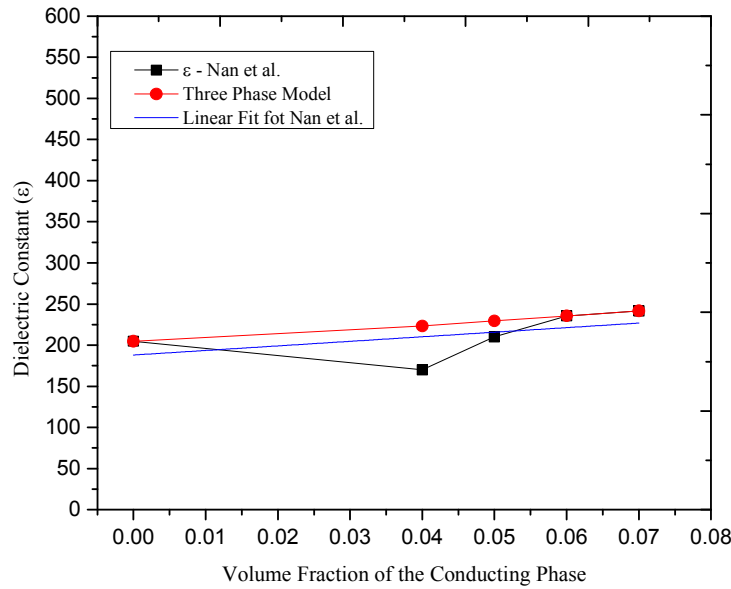


Figure 2-5 Comparison of the dielectric Constant of the Terfenol D-PZT-PVDF composite [58,111] with Equation (2.6). The figure also shows that the model has a similar trend to that of the linear best fit of the experimental data

In order to examine the influence of conductive inclusion shape on the effective dielectric constant of the composite, we have used our model Equation (2.8) to predict these values for the BaTiO₃- PVDF- MWCNT (multi walled carbon nanotube inclusions as conductive

inclusions in the composite). A comparison of the three phase model with the values of the dielectric constant of the three phase BaTiO₃-PVDF-MWNT (multiwalled carbon nanotube) is shown in Figure 2-6. Here, the spheroidal conductive inclusions are MWNTs. The predicted values from the three

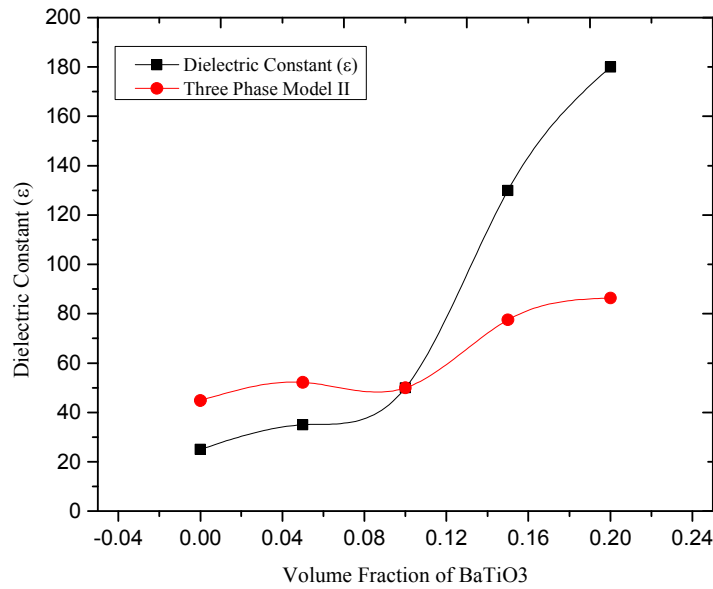


Figure 2-6 Comparison of the dielectric Constant of the BaTiO₃-PVDF-MWNT composite [111,113] with an average MWCNT aspect ratio of 10, with Equation (2.8)

phase model compares well with the experimental data except for BaTiO₃ volume fractions of 0.15 and 0.20 where the variation can be attributed to MWNT polarization, which the model does not take into account [77,109].

2.3 Conclusions

Analytical expressions for the estimation of the effective dielectric constant of a 0-3-0 composite have been derived for both spherical and spheroidal conductive inclusions. Here, we consider the 0-3 composite as an isotropic material and then evaluate the effective dielectric constant of the 0-3-0 composite by assuming spherical/spheroidal inclusions of the third phase in the 0-3 composite matrix. The derived expression for the spherical conductive inclusion is validated favorably with experimental values from Nan et al. [58]. The analytical model is compared to experimental results where the conductive filler material is comprised of micron sized particles. However, the influence of conductive material particle size on the effective dielectric constant is yet to be determined. A comparison of the analytical predictions with the experimental values from Yao et al. [78], validates the three phase analytical model for 0-3-0 composites with spheroidal conductive inclusions. Future work will include the extension of the above analytical model to estimate the piezoelectric strain coefficient.

Chapter 3.

Effect of PZT volume fraction and Al inclusions on three phase 0-3-0 PZT-Epoxy-Al composites

As dielectric materials, two-phase 0-3 composites have relatively low values of dielectric constant as compared to three phase 0-3-0 composite piezoelectric materials; which are comprised of piezoelectric and electrically conductive particles embedded within a continuous matrix [32,33,77]. Thus, in order to enhance the dielectric properties of two-phase polymer-based composites, researchers have investigated three phase composites consisting of a piezoelectric ceramic, metal, and polymer. Choi et al. [38] found that BaTiO₃–PMMA-Ni composites comprised of 10% volume fraction of nickel (40 nm in size) had dielectric constants equal to ~ 110 compared to the two-phase CPP, BaTiO₃–PMM, which had a dielectric constant equal to ~ 14.4 [25]. In addition to higher dielectric constants, these three phase composites have low processing temperatures [24] and improved loss factors, which make them suitable for damping materials [32,63,65,66,77,78].

The dielectric behavior of the composites is dependent upon the size, shape, and spatial distribution of the filler particles within the host matrix, the adhesion and the interaction between the phases, and the processing method [32, 38, 39, 68, 79,104, 106, 118]. In this chapter, we report on the effects of the conductive particle inclusions on the dielectric properties of the PZT (piezoelectric)-epoxy-Aluminum (conductor) composite.

Specifically, the influence of the spherical Al inclusions on the dielectric constant, strain coefficient and $\tan \delta$ is observed. The PZT-epoxy-Al composites examined comprised of micron and nanosize aluminum particles.

Two and three phase epoxy/piezoelectric/conductive filler composites were fabricated. The volume fraction of the conductive filler, Aluminum, was held constant at 20%, while the volume fraction of the piezoelectric material, PZT was varied from 0.10 to 0.70 [110, 116]. The influence of the aluminum inclusions and the PZT volume fraction on the dielectric properties of the three phase PZT-epoxy-aluminum composites was experimentally investigated. The influence of the Aluminum volume fraction was also studied, by varying the Aluminum volume fraction from 1% to 20% and keeping the PZT volume fraction constant at 30%. In general, dielectric and piezoelectric properties of the PZT-epoxy matrix were improved with the addition of Aluminum particles. Three sets of composites were examined, wherein, the size of the Aluminum inclusions were micron in size (200 mesh). The three phase composites presented enhanced dielectric constant, loss factor ($\tan \delta$) and piezoelectric coefficient (d_{33}) as compared to the two phase 0-3 composites with the same PZT volume fractions. The fabrication of two phase 0-3, and three phase 0-3-0 composites and the influence of the micron sized Al inclusions has been discussed in this chapter.

3.1. Fabrication of two phase 0-3 PZT-Epoxy composites

The active piezoelectric material used was PZT, EC-76 R8658 from Reade International with average particle size of 6 μm (sizes range from 2 – 7 μm). Table 3-1 presents the nominal physical characteristics of the PZT used. The epoxy used was DGEBA, Epofix Cold-Setting Embedding Resin from Electron Microscopy Sciences. The epoxy density (in the wet-state) was 1.16 g/cm^3 . PZT which is ball milled for 1 hour is added to epoxy. The PZT volume fraction varied from 1% to 70%. This mixture is then dispersed in ethanol and sonicated till the ethanol evaporates. The mixture is then mixed with the DGEBA curing agent (DGEBA hardener from the Epofix Cold Setting Embedding Resin). This is then sonicated for 30 minutes. The final mixture was then poured into a circular mold that was 6 mm thick and with a radius equal to 7.5 mm. The mold, containing the sample, was placed in between the top and bottom platens of a Carver Hydraulic press, and subjected to 500 psi for 5 min at room temperature. The samples were then cured at 75⁰ C for 8 hours. The samples were polished and subsequently painted on the top and bottom surfaces with conductive silver paint. They were then poled at 0.2 kV/mm at 120⁰ C for 10 minutes in silicone oil, using the Spellman High Voltage Generator and the high voltage contact poling fixture as shown in Figure 3-1. After poling, the sample was wrapped in Aluminum foil for 24 h to get rid of residual charges on the surface of the samples. The samples were then tested for their electromechanical properties [110, 116].

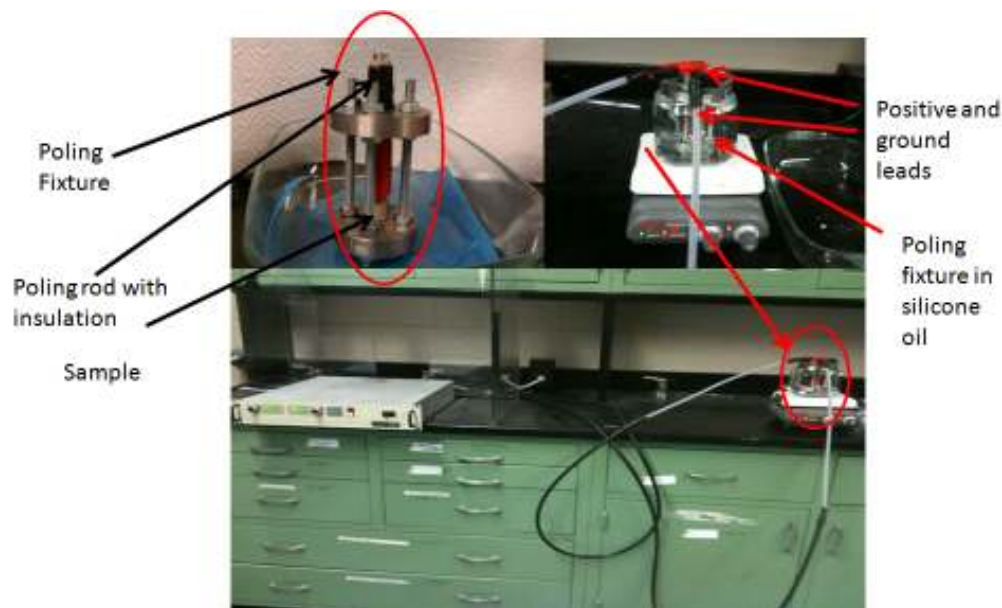


Figure 3-1 Spellman high voltage generator and the high voltage poling fixture used in the contact poling of the two phase 0-3 and three phase 0-3-0 composites

Table 3-1
Physical properties of PZT, EC76.

Physical Property	Metric
Density	7.0–8.0 g/cc
Young's Modulus	50.5 GPa
Piezoelectric Coefficient, d33	425–500 pC/N

3.2 Fabrication of three phase 0-3-0 PZT-Epoxy-Al micron sized composites

The fabrication technique for the three phase 0-3-0 composites were similar to that of the two phase 0-3 composites as shown in Figure 3-2. The PZT and Epoxy used were similar to that used for the two phase composites. The micro size Aluminum (200 mesh) was 99.97% purity grade, Nitrogen flushed, and purchased from Acros Organics, with true density equal to 2.69 g/cm^3 . The morphologies of the individual phases, micron size Aluminum, PZT, and the epoxy matrix are shown in Figure 3-3 A), B), C) respectively.

In particular, Figures 3-3 A), B) and C) depict spheroid shaped micron sized Al inclusions, spherical shaped PZT and the uniform Epoxy matrix.

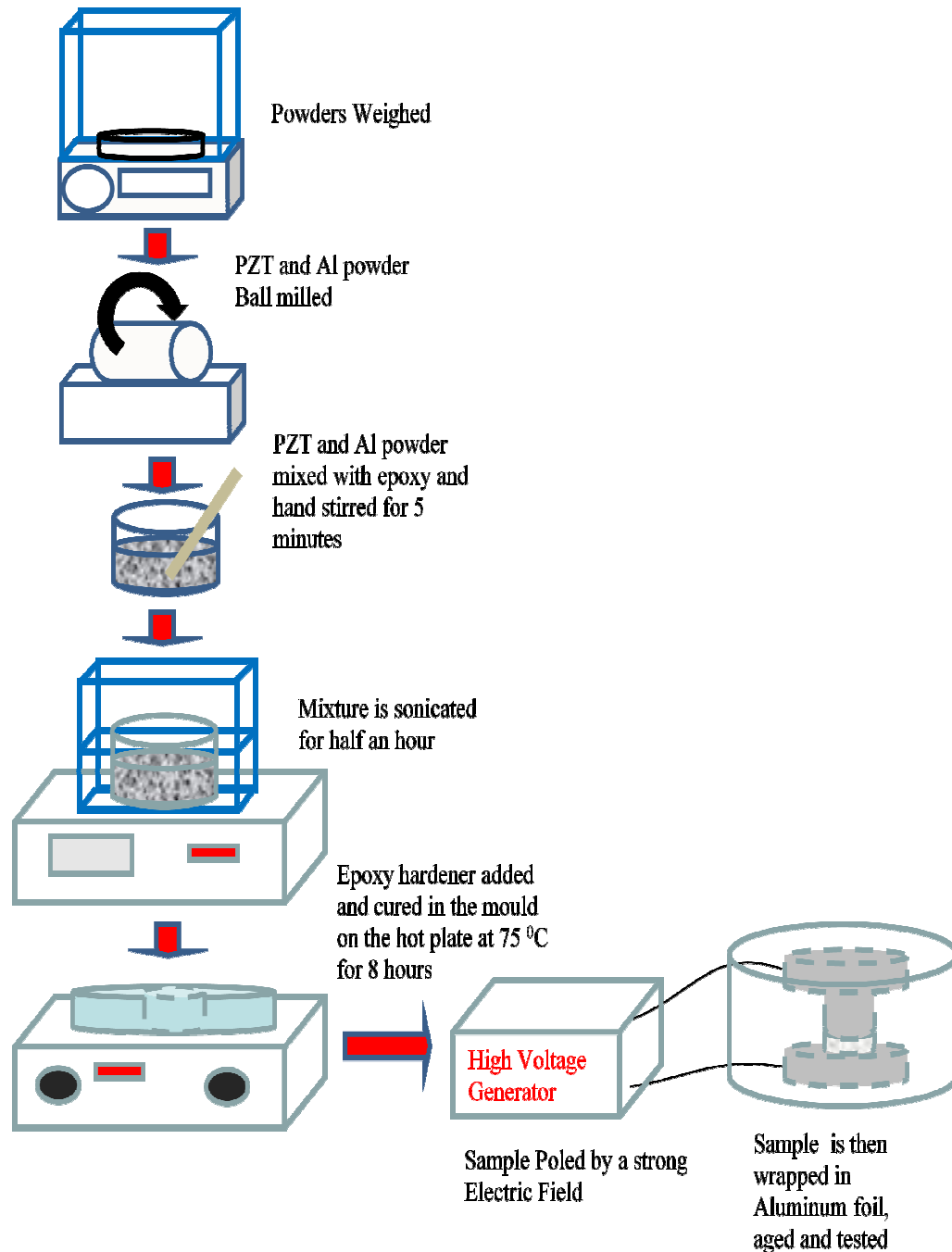


Figure 3-2 Experimental procedure for fabrication of three phase 0-3-0 PZT-Epoxy-Al composites

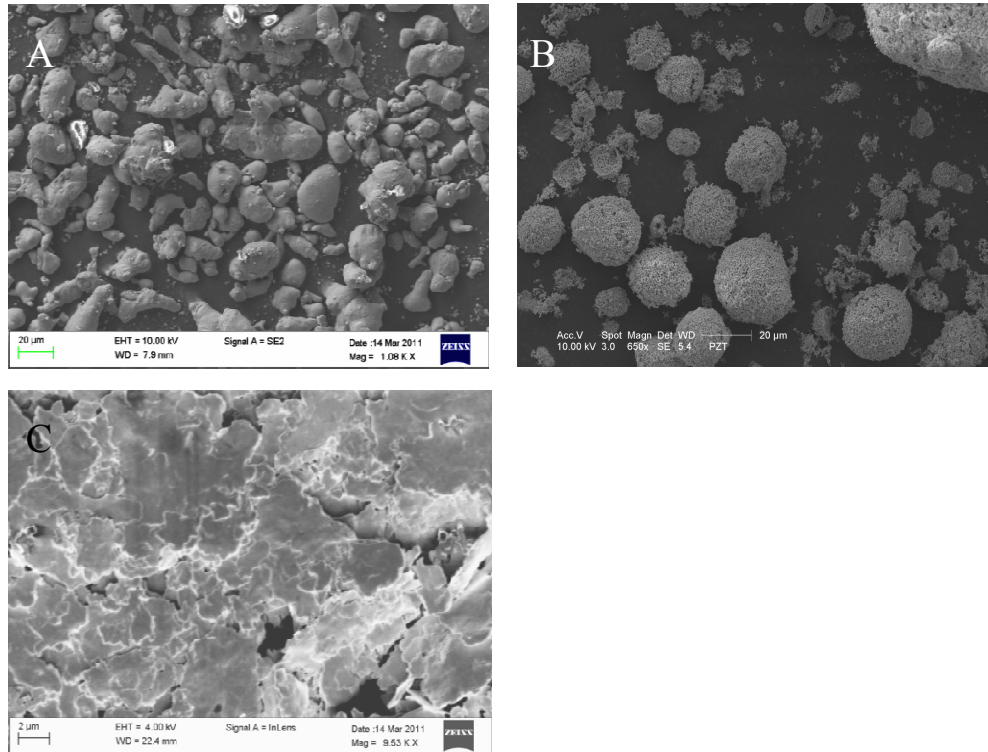


Figure 3-3 Morphologies of the individual phases of the 0-3-0 composite as seen in the SEM micrographs, A) Micron sized Al inclusions, B) PZT particles, and C) Epoxy Matrix

The fabrication procedure involves several steps as depicted in the Figure 3-2. Aluminum particles were dispersed in ethanol and stirred in a sonicator for 30 minutes. The volume fraction of the aluminum was held constant at 20%, while the volume fraction of PZT was varied from 0.10 to 0.70 (10% - 70 %). The PZT was ball milled for 1 hour and then mixed with epoxy. This mixture was then stirred for 10 minutes. The PZT-Epoxy mixture was then added to the dispersion of Aluminum in ethanol and then stirred in an ultrasonicator until the ethanol is evaporated. The mixture was then combined with the

DGEBA curing agent and sonicated for 30 minutes. The mold, containing the sample, was placed in between the top and bottom platens of a Carver Hydraulic press, and subjected to 500 psi for 5 min at room temperature, and then allowed to cure at 75⁰ C on a hot plate for 8 hours. The samples were then polished and painted on the top and bottom surfaces with conductive silver paint. They were nominally 15 mm in diameter and 6 mm in thickness. In order to sufficiently and safely pole the samples, a special fixture was fabricated in-house to eliminate the need for external wire attachment to the samples. This fixture and the poling set-up are provided in Figure 3-1. The samples were poled at 0.2kV/mm, in a silicon bath at 120⁰ C for 10 minutes and then then quenched in cold silicon for fast cooling. They were then wrapped in aluminum foil and allowed to cure for 24 hours prior to acquisition of data. Three samples were prepared for each volume fraction of PZT.

3.3 Experimental results and discussions

Two-phase PZT-epoxy composites were fabricated, where the volume fraction of PZT was varied from 10% to 70%. The dielectric constant of the two-phase composite is plotted as a function of volume fraction of PZT as shown in Figure 3-4. As expected, the dielectric constant of the composite increased with the volume fraction of PZT. The dielectric constant plot as a function of piezoelectric volume fraction followed the same trend as Ref. [79] and [106], wherein the results fall between the Maxwell Garnett approximation and the Bruggeman's effective medium approximation [79].

$$\varepsilon = \varepsilon_{Epoxy} \left[1 + \frac{1 + 3\phi_{PZT}\beta}{1 - \phi_{PZT}\beta} \right] \quad (3.1)$$

$$\varepsilon = (1 - \phi_{Inclusion}) \frac{\varepsilon_{Matrix} - \varepsilon}{\varepsilon_{Matrix} + 2\varepsilon} + \phi_{Inclusion} \frac{\varepsilon_{Inclusion} - \varepsilon}{\varepsilon_{Inclusion} + 2\varepsilon} \quad (3.2)$$

Here ϕ_{PZT} is the volume fraction of PZT, $\beta = \varepsilon_{PZT} - \varepsilon_{Epoxy} / \varepsilon_{PZT} + 2\varepsilon_{Epoxy}$, and ε , ε_{PZT} , and ε_{Epoxy} represent the dielectric constant of the two-phase composite, PZT and epoxy, respectively. Both analytical models can be used to determine the effective dielectric constant of a matrix-based composite with embedded inclusions [79]. In general, the Maxwell expression underestimates [79] the effective dielectric constant, while Bruggeman's expression overestimates this value as the volume fraction of the piezoelectric inclusion increases.

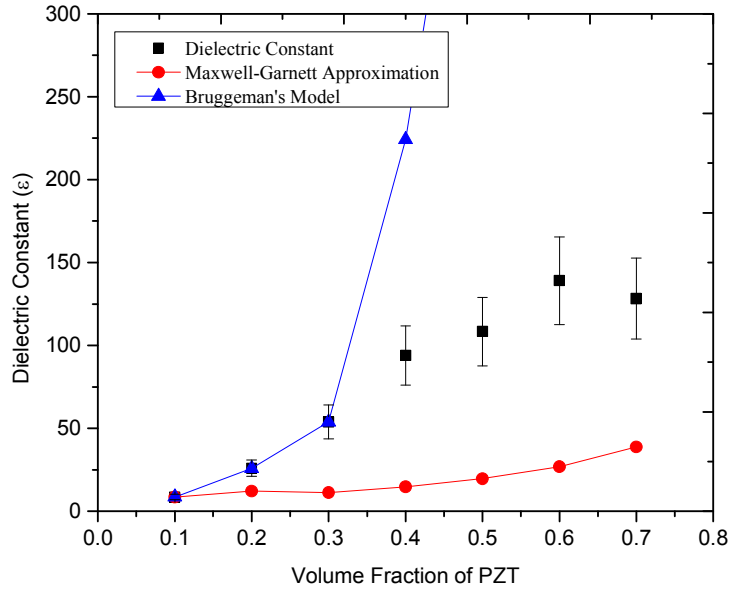


Figure 3-4 Comparison of the dielectric constant (ε) of the two phase 0-3 composite with effective dielectric constant models, namely the Maxwell-Garnett approximation and the Bruggeman's Model, shows the Maxwell-Garnett's model

underestimates and the Bruggeman's model overestimates the predicted values of the effective dielectric constant

For our data, the Maxwell expression underestimates and Bruggeman's expression overestimates the empirical results for PZT volume fractions $>30\%$ as shown in Figure 3-4. This is due to the aggregation of PZT and epoxy particles in the composite along with the increase in PZT volume fraction, which results in continuous percolation clusters in the composites [79]. A SEM image that details the distribution of PZT within the epoxy matrix is provided in Figure 3-5. The SEM micrograph of the PZT-Epoxy two phase composite is magnified 5000 times. The arrows indicate the PZT and epoxy matrix in the microstructure. Evidence of PZT clustering is seen, which supports the explanation for the underestimation of the Maxwell Garnett approximation.

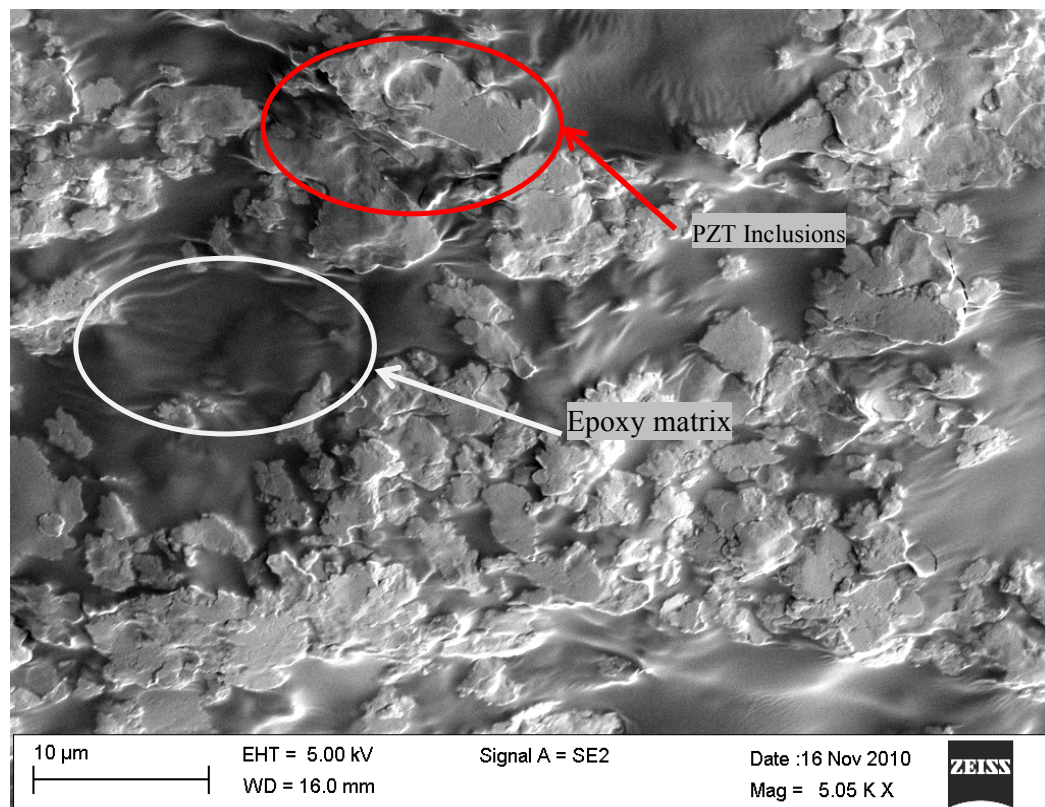


Figure 3-5 SEM micrograph of a two phase PZT-Epoxy composite showing the distribution of the PZT particles in the Epoxy matrix with PZT volume fraction at 30 %

In Fig. 3-6, a plot of the effective dielectric constant as a function of PZT volume fraction is provided for the PZT-epoxy and the three phase composites with micron sized Aluminum inclusions. The volume fraction of the Al inclusions is held constant at 20% for all three phase composites. As expected, the dielectric constants of the three phase composites are greater than those of the two phase PZT-epoxy composites. This is attributed to the increase in the effective dielectric constant by the addition of the aluminum particles. This enhancement can be explained by the following power law [38, 79]:

$$\varepsilon_{ThreePhase} = \varepsilon \left| \frac{\phi_c - \phi}{\phi_c} \right|^{-q} \quad (3.3)$$

Where ε is the dielectric constant of the PZT-Epoxy two phase composite, ϕ_c is the volume fraction of Aluminum at the percolation threshold, ϕ is the volume fraction of Aluminum in the composite, and q is the critical exponent. A value of 1.3 was determined for the critical exponent, q , when the value for ϕ_c is estimated as 16% [79,106] and the experimental values for the dielectric constant were substituted into Equation (3.3).

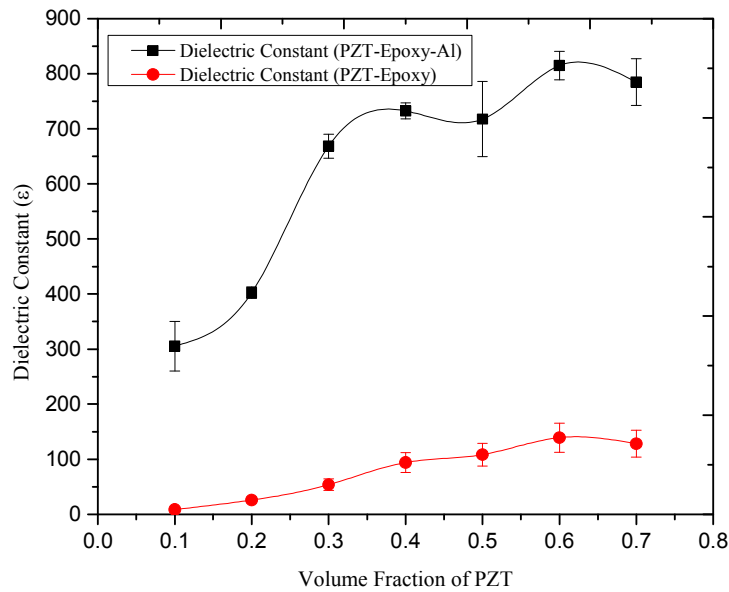


Figure 3-6 Comparison of the Dielectric Constant (ϵ) of the two phase PZT-Epoxy and three phase PZT-Epoxy-Al composites

The effective dielectric constant for the composite that incorporates micro-size aluminum particles presents higher effective dielectric constants for equivalent volume fractions of PZT than the two phase composites. For example, at volume fractions of 20%, 30%, and 40% of PZT, the dielectric constants of the micro-composites are 405.74, 661.38, and 727.78 as compared to 25.99, 53.90, and 93.98, respectively, for the two phase composite. Differences in the piezoelectric strain coefficient and loss factor, $\tan \delta$, are also observed when aluminum particles are added to the two-phase composite. $\tan \delta$ is an important parameter in the characterization of the macromolecular viscoelasticity of the material. It represents the damping capacity of the material and describes the ability of the material to convert mechanical energy into heat energy, when subjected to an external load. The results provided in Figure 3-7 indicate that all of the composites show an increase in loss

factor at higher concentrations of PZT. This trend agrees well with those noted by Refs. [65] and [81]. The composites that have the micron size Aluminum particles present higher values of $\tan \delta$ than the two phase composites. For example, the $\tan \delta$ values for a PZT volume fraction equal to 70% are 0.014, and 0.0457 for the PZT-epoxy, and PZT-epoxy-Al micro-composites, respectively.

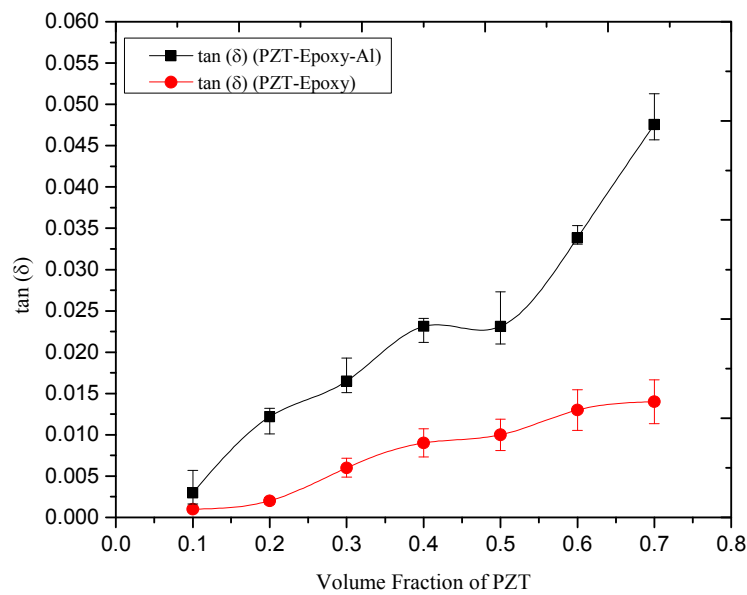


Figure 3-7 Comparison of the $\tan(\delta)$ of the two phase PZT-Epoxy and three phase PZT-Epoxy-Al composites

In Fig. 3-8, a plot of the piezoelectric strain coefficient, d_{33} , as a function of PZT volume fraction is presented. As evidenced by other researchers [92, 102], d_{33} increases with the volume fraction of PZT in composite piezoelectric materials. The strain coefficient is a function of effective dipole moment in the direction of the energy generation under an applied Mechanical deformation. The increase in volume fraction of the piezoelectric ceramic, PZT, increases the strength of the effected electric field generated under applied

strain which in turn increases the piezoelectric strain coefficient.

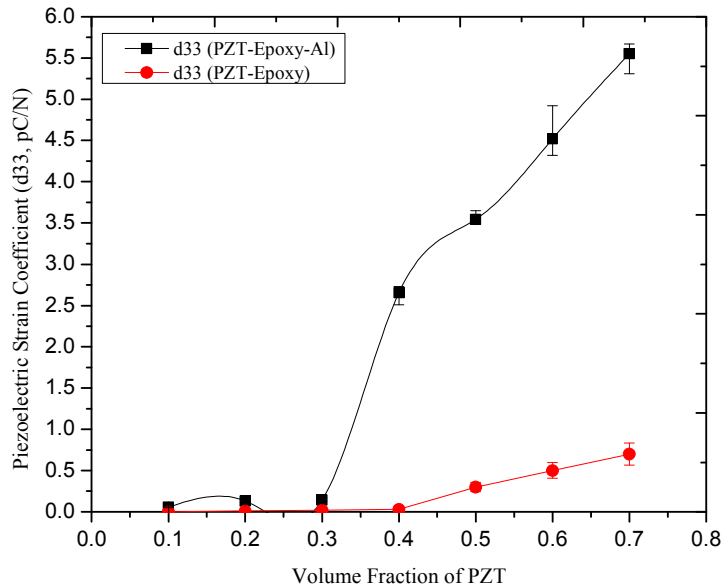


Figure 3-8 Comparison of the piezoelectric strain coefficient, d_{33} of the two phase PZT-Epoxy and three phase PZT-Epoxy-Al composites

Figure 3-9 shows the distribution of the Aluminum and PZT inclusions in the 3-dimensional Epoxy matrix. The SEM micrographs show evidence of clustering of PZT inclusions embedded in the epoxy matrix. The Aluminum inclusions also show signs of agglomeration which increases the effective particle size of the Aluminum inclusions. Composite homogeneity is a critical parameter in achieving optimal performance and is a challenge to achieve due to space charge effects. Adequate dispersion of PZT and conductive filler within the polymer matrix, and minimal air voids are desirable. However, agglomeration of PZT and conductive filler material within the matrix is common [66] as evidenced by the SEM images. The agglomeration of the constituent materials can lead to reduced mechanical, electrical, and conductive properties in the materials.

Agglomeration was observed in all of the sets of composite materials. Also, addition of ceramic materials tends to introduce flaws, in the form of agglomerations that contribute to scattering of results [66].

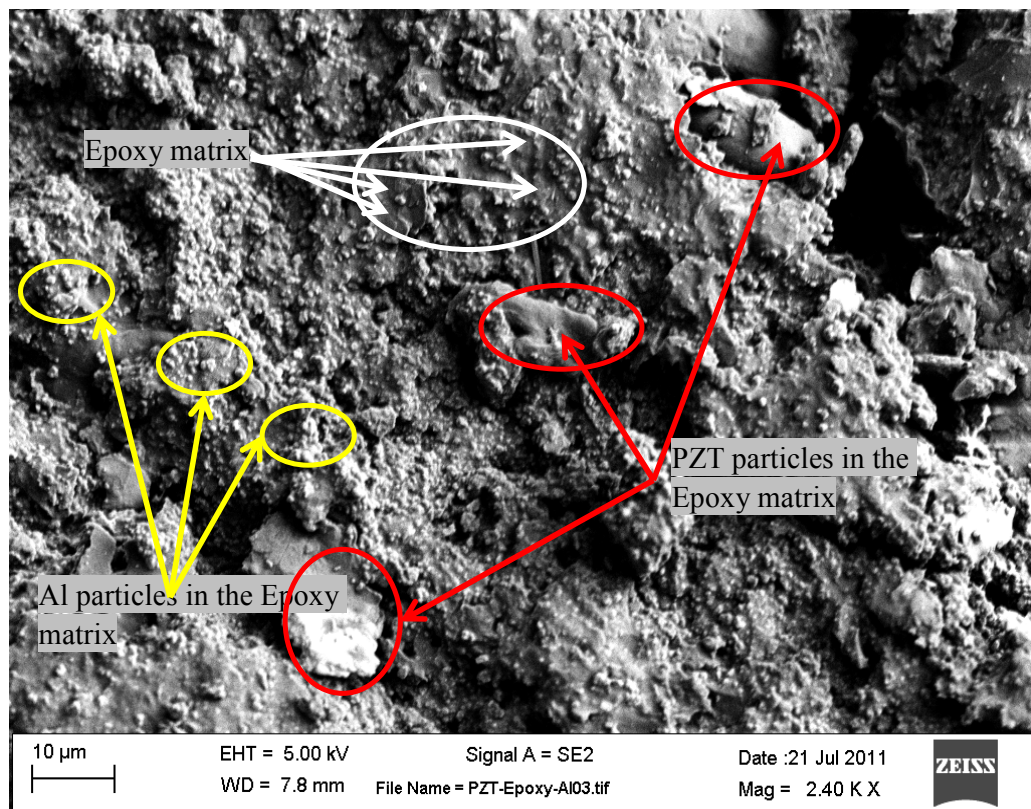


Figure 3-9 SEM micrograph of a three phase PZT-Epoxy-Al micro composite showing the distribution of the PZT particles and micron sized Al inclusions in the Epoxy matrix with PZT volume fraction at 50 % and Al volume fraction at 20 %

3.4 Three phase PZT-Epoxy-Al composite with varying Al volume

fraction

Three phase PZT-Epoxy-Al composites were fabricated. The fabrication technique for the three phase 0-3-0 composites with varying Aluminum volume fraction, was the same as used before for the three phase composites and shown in Figure 3-2. The volume fraction of the PZT is kept constant at 30% and the Aluminum volume fraction is varied from 1% to 20%. The d_{33} values increase with increasing Aluminum volume fraction which can be attributed to the increase in polarization of the composite with increasing Aluminum volume fraction [33, 38, 39, 63]. This increase is seen till the material reaches the percolation threshold around an Aluminum volume fraction of 16%. The d_{33} values have reach a maximum 1.12 pC/N, and then dips down to 0.13 pC/N for an increase in Aluminum volume fraction from 17% to 20%, as shown in Figure 3-10. A similar trend is seen for the dielectric constant of the composite, which increases from ~24 to ~191, when the volume fraction of the Aluminum inclusions is increased from 1% to 17%, as shown in Figure 3-11. When the composite reaches the percolation threshold an abrupt increase in the dielectric (~739) is observed.

This sharp increase in the dielectric constant and the decrease in the piezoelectric strain coefficient is called as the smearing region [33, 38, 39], where the individually isolated conductive particles or conductive particle clusters are moved to infinitely connected percolation clusters.

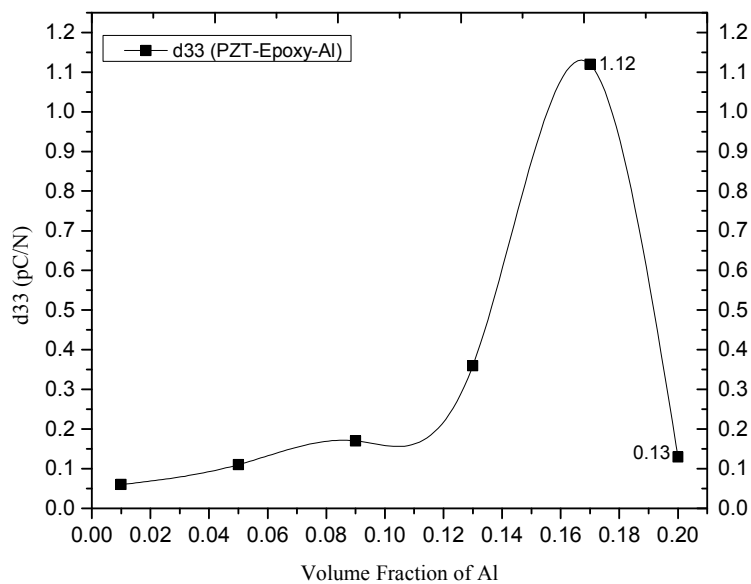


Figure 3-10 Variation of the piezoelectric strain coefficient, d_{33} as a function of increasing Al volume fraction

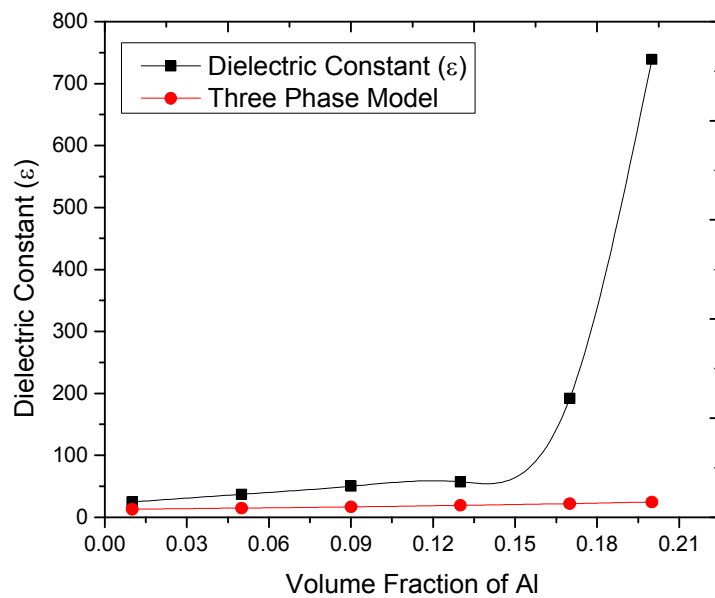


Figure 3-11 Variation of the dielectric constant, ϵ of the three phase composite with varying Al volume fraction and comparison with the three phase model

A comparison of the dielectric constant with the prediction from the three phase model [109,125] (Equation 2.5, Chapter 2) shows that the experimental results deviate from the model when the composite reaches the percolation threshold after an Al volume fraction of 13%. This can be attributed to the fact that the three phase model does not take into consideration the percolation phenomenon in the composite. The variation of the dielectric loss, $\tan \delta$ of the three phase composite with the increase in the Aluminum volume fraction is also demonstrated in Figure 3-12 for PZT Volume fraction of 0.3. As expected the $\tan \delta$ increases with the increase in the Aluminum volume fraction and a similar trend is observed beyond the percolation threshold, where the formation of infinitely long percolation clusters contribute to the increase in the loss tangent.

Figure 3-13 shows the distribution of the PZT and Aluminum inclusions in the Epoxy matrix at an Al volume fraction of 17%. It shows the presence of Aluminum agglomerations and the formation of continuous percolation pathways surrounded by PZT clusters. The SEM micrograph along with the d_{33} and dielectric constant measurements show that the percolation threshold for the PZT-Epoxy-Al three phase composite lies around an Al volume fraction of 13% - 17% with the PZT volume fraction held constant at 30%.

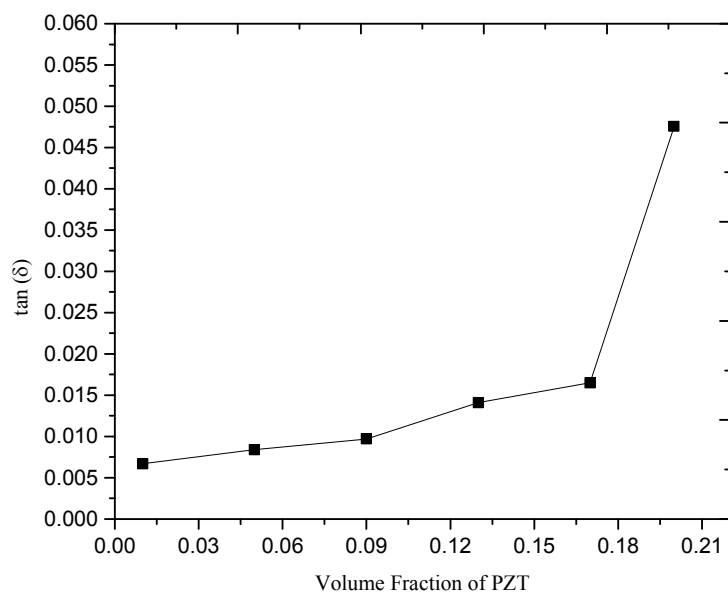


Figure 3-12 $\tan(\delta)$ of the three phase PZT-Epoxy-Aluminum composite with varying Aluminum volume fraction with PZT volume fraction of 0.3

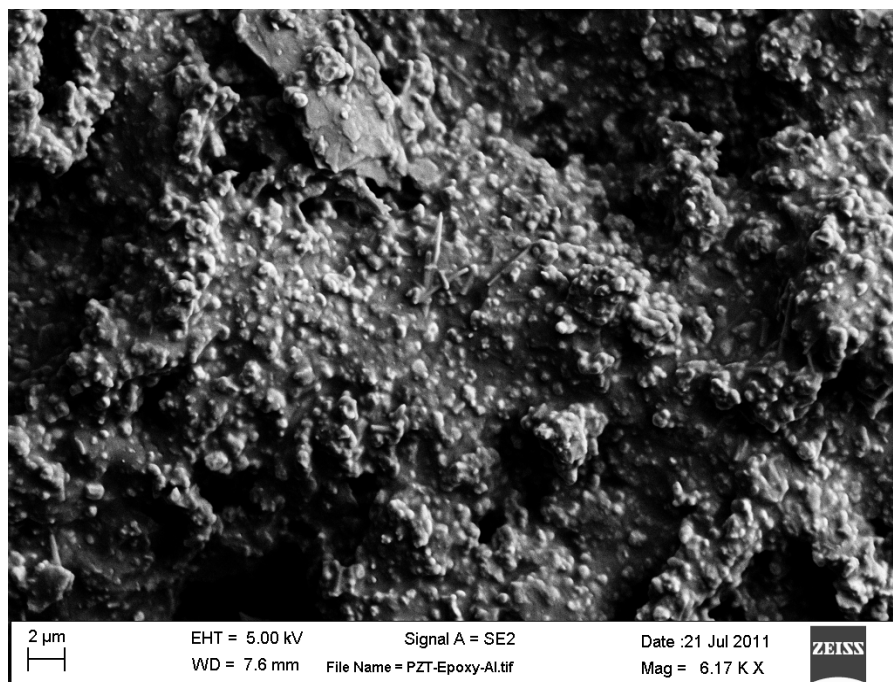


Figure 3-13 SEM micrograph of a three phase PZT-Epoxy-Al micro composite showing the distribution of the PZT particles and micron sized Al inclusions in the

Epoxy matrix with PZT volume fraction at 30 % and Al volume fraction at 17 %

According to Choi et al. and Dang et al. [39, 80] the percolation threshold will change with the change in the PZT volume fraction. The same phenomenon is seen for the three phase PZT-Epoxy-Al composites when the PZT volume fraction is reduced from 30% to 20%. For a PZT volume fraction of 20% the peak d_{33} value for the composite is reached at an Al volume fraction of 9% as opposed to that of 17%, when the PZT volume fraction is 30%, as shown in Figure 3-14.

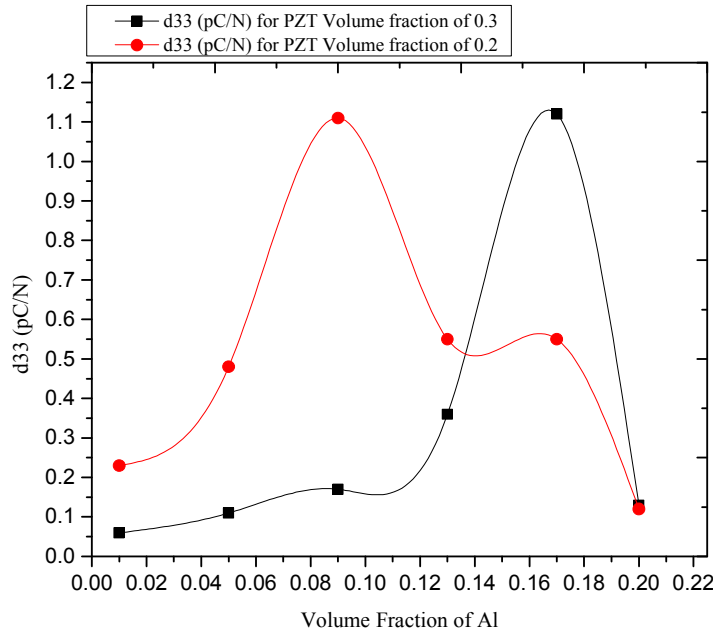


Figure 3-14 Variation of the percolation threshold as demonstrated by the change in d_{33} as a function of varying Al volume fraction, along with the change in PZT volume fraction from 20% to 30%

This peak is followed by a drop in d_{33} values for each set of composites. A similar phenomenon is observed in Figure 3-15 where the dielectric constant jumps up from ~ 35 to ~ 91 when the Al volume fraction changes from 9% to 13% and the PZT volume fraction is held constant at 20%. On the other hand this drastic increase in the dielectric

constant is observed at an Al volume fraction of 17% for the three phase composite with the PZT volume fraction constant at 30%. This indicates that the percolation threshold increases with an increase in the PZT volume fraction.

This can be explained by hypothesis that the PZT inclusions impede the formation of the Al percolation clusters [38, 39, 79]. This is due to the fact that individual an agglomerated Al particles are surrounded by the PZT clusters which hinders the formation of the percolation pathways thus increasing the percolation threshold with increasing PZT volume fraction. This phenomenon can also be seen in the SEM micrographs in Figure 3-9 and 3-13. This allows us to tailor the piezoelectric and dielectric properties of the three phase composite by broadening or narrowing the smearing region and the percolation threshold according to the requirements in embedded systems, energy harvesting and sensor based devices.

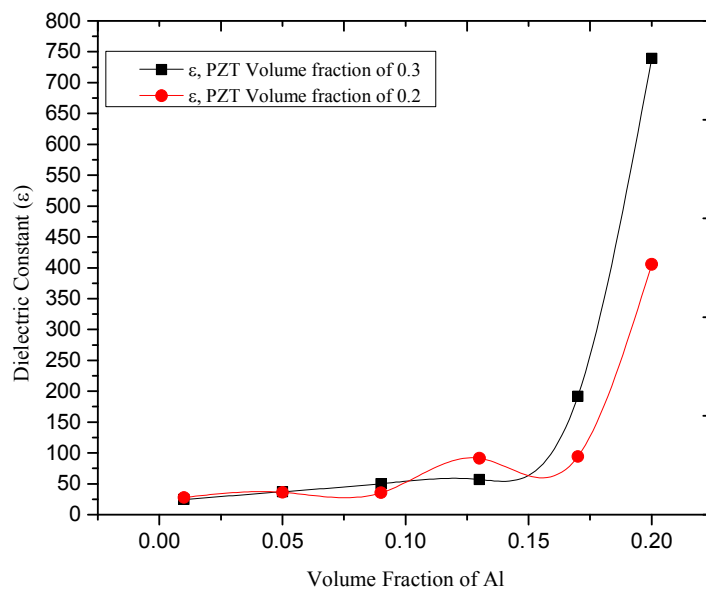


Figure 3-15 Variation of the percolation threshold as demonstrated by the change in

3.5 Conclusions

Piezoelectric composites comprised of PZT, Epoxy, and Al were fabricated, and the volume fraction of the PZT and Aluminum were varied to study the effect on the variation of the effective piezoelectric and dielectric properties. The dependence of the dielectric and piezoelectric characteristics of the composite on the volume fraction of PZT has been established. The enhancement of dielectric and piezoelectric properties resulting from the addition of Al inclusions and increase of PZT volume fraction has been shown. A comparative study of the variation of the percolation threshold and the smearing region by changing the PZT and Al volume fraction has also been demonstrated. The variation in properties, prove that the dielectric and piezoelectric characteristics of these particulate composites can be tailored by varying the PZT and Al volume fractions, while the other parameters remain fixed. The ease of processing, flexibility, and good dielectric behavior of the three-phase piezoelectric particulate composites potentially makes the composites suitable for practical applications in energy harvesting, acoustic dampening, embedded systems and structural health monitoring applications.

Chapter 4.

Effect of PZT volume fraction and the size of Al inclusions on three phase 0-3-0 PZT-Epoxy-Al percolative composites

The size of the piezoelectric particles within the composite also has an influence on the dielectric constant of the three phase composites. The dielectric constant of the three phase CPP [39,39, 79], BaTiO₃–PMMA–Ni comprised of micron size BaTiO₃ particles was found to be 150, in comparison to 100 for three phase composites with nanosize BaTiO₃ particles. The effects of the piezoelectric particle size on the bulk properties of the composite was attributed to the increase in percolation threshold of nickel that was caused when individual or aggregate BaTiO₃ particles surrounded the nickel particles [79]. The dielectric behavior of the composite is dependent upon the size, shape, and spatial distribution of the filler particles within the host matrix, the adhesion and the interaction between the phases, and the processing method [32, 38, 39, 68, 79,104, 106, 118]. In this chapter, we report on the effects of the size of the conductive particle on the dielectric properties of the piezoelectric-epoxy-conductor composite. Specifically, the influence of the size of the Aluminum particle on the dielectric constant, strain coefficient and $\tan \delta$ is observed. The PZT-epoxy-Al composites examined comprised of micron and nanosized Aluminum particles.

4.1 Fabrication of two phase 0-3 PZT-Epoxy composites

Three sets of composites were examined, wherein, the size of the Aluminum inclusions were varied from micron in size (200 mesh) to nano in size (~18 nm). The nano Aluminum particles were uncoated and were of 99.9% purity, APS 18 nm grade from Materials Tech International, bulk density equal to $0.08 - 0.2 \text{ g/cm}^3$ and true density equal to 2.64 g/cm^3 . The morphology of the individual phase of the nano sized Aluminum (at 8.25K magnification and at 108.69K magnification) in clusters (clouds), are shown in Figures 4-1 A) and B) respectively. In particular, Figures 4-1 B) depicts the spherical shaped nano sized aluminum particles. The experimental process for the fabrication of the three phase PZT-Epoxy-Al nano composites was similar to that of the micron sized composites as shown in Figure 3-3 of Chapter 3. Aluminum particles were dispersed in ethanol and stirred in the sonicator for 30 min. The volume fraction of the aluminum was held constant at 20%, while the volume fraction of PZT was varied from 0.10 to 0.70. The PZT and epoxy were mixed separately and stirred for 10 min, and then ball milled for 1 hour. The aluminum, PZT and epoxy/ethanol were then combined and subjected to ultrasonication until the ethanol evaporated. The mixture was then combined with the DGEBA hardener and sonicated for 30 min. The final mixture was poured into a mold and hand pressed for 5 min, and then allowed to cure at 75°C on a hot plate for 8 hours. Samples were then polished and painted on the top and bottom surfaces with conductive silver paint [110, 116].

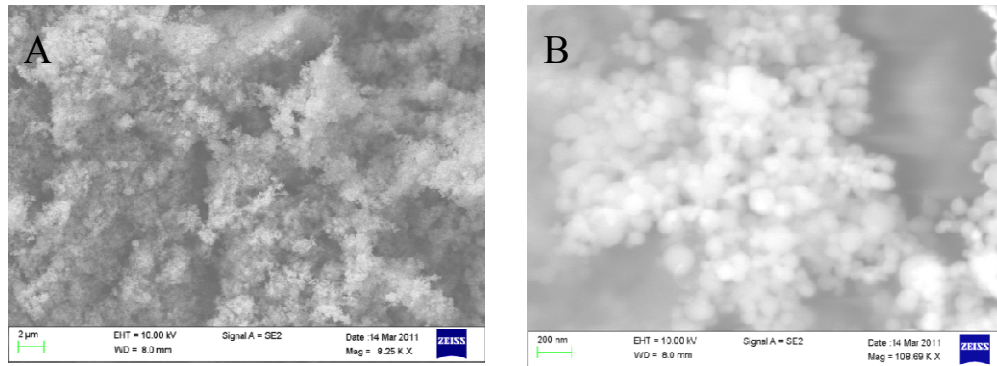


Figure 4-1 SEM micrographs of Al nanopartilces showing A) Clusters of Al nanoparticles and B) Spherical nano-particles

The samples were nominally 15 mm in diameter and 6 mm in thickness. The samples were poled at 0.2 kV/mm, in a silicon bath at 120⁰C for 10 min. The samples were then quenched in cold silicon for fast cooling. The samples were then wrapped in aluminum and allowed to age for 24 hours prior to acquisition of data.

4.2 Experimental results and discussions

The strain coefficient, d_{33} , dielectric loss factor, $\tan \delta$ and the dielectric constant, ϵ were measured using a Piezo Meter System manufactured by Piezo Test, Piezoelectric Materials & Device Testing Company. Specifically, composites comprised of micron sized aluminum particles and PZT volume fractions of 20%, 30%, and 40% had dielectric constants equal to 405.7, 661.4, and 727.8 respectively (as shown in Figure 4-2), while composites comprised of nanosized Aluminum particles with the same PZT volume fractions, had dielectric constants equal to 233.28, 568.81, and 657.41, respectively as shown in Figure 4-2. The dielectric constant values are also compared to the percolation

model as shown in Equation 3.3 with a critical exponent of 1.3.

Composites having micron size aluminum particles exhibited higher loss factor and strain coefficients than those that incorporated nano size aluminum particles, which could be due to several factors: agglomeration, contact resistance between particles, and excess air voids in the samples.

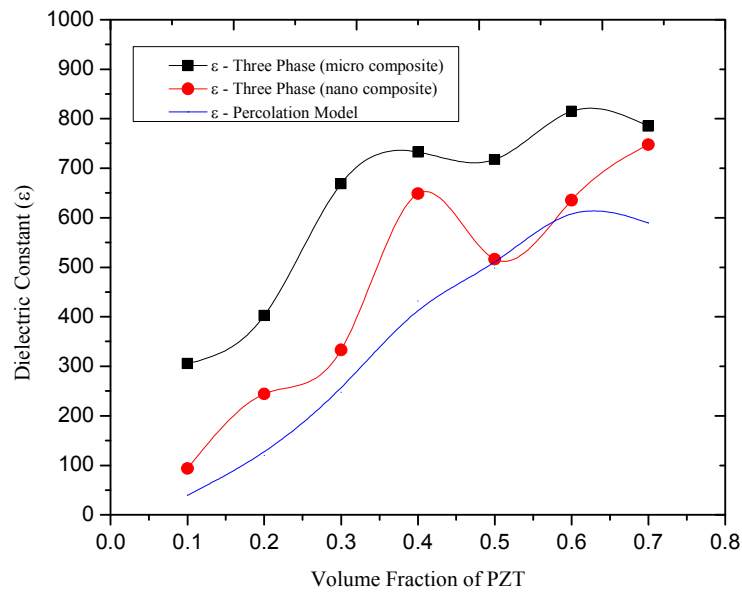


Figure 4-2 A comparison of the dielectric constant of three phase micro and nano composites along with the percolation model for the dielectric constant

A plot of the composite dielectric loss factor ($\tan \delta$) as a function of PZT volume fraction is presented in Figure 4-3. The results provided in Figure 4-3 indicate that both sets of composites show an increase in loss factor at higher concentrations of PZT. This trend agrees well with those noted by [65, 66]. The composites that have the micron size aluminum particles present higher values of $\tan \delta$ than the corresponding composites with nano-size aluminum constituents. This trend also agrees well with those noted by [65, 66].

The experimental values also follow the power law [38]:

$$\tan \delta = \tan \delta_0 \left| \frac{\phi_c - \phi}{\phi_c} \right|^{-r} . \quad (4.1)$$

In Eq. (4.1), $\tan \delta$ is the dielectric loss tangent of the two phase matrix and r is direct current conductivity of the composites. The experimental values of the dielectric loss tangent are in good agreement with Eq. (4.1) and follow the same trend as [79, 106]. The coefficient, r may be determined from the empirical data provided. In Fig. 4-2, the empirical data is plotted against the power law for the loss tangent of micro and nano-three phase composites with r of 1.2 and 2.5 respectively.

In Figure 4-4, a plot of the piezoelectric strain coefficient, d_{33} , as a function of PZT volume fraction is presented. As evidenced by other researchers [90, 106], d_{33} increases with the volume fraction of PZT in composite piezoelectric materials. Similar to the loss factor results presented in Figure 4-3, the strain coefficient of the composites containing nano-size particles of aluminum are lower than those containing micron size particles of aluminum. The strain coefficient is a function of the Capacitance of the material, which is proportional to the number of charges that are stored on the surface of the sample under an applied electric field. The inclusions of the Aluminum fillers within the PZT/epoxy composite, result in higher permittivity of the composite, and ultimately higher piezoelectric coefficients. Increases in the piezoelectric coefficient, d_{33} are observed for both sets of composites above 30% volume fraction of PZT.

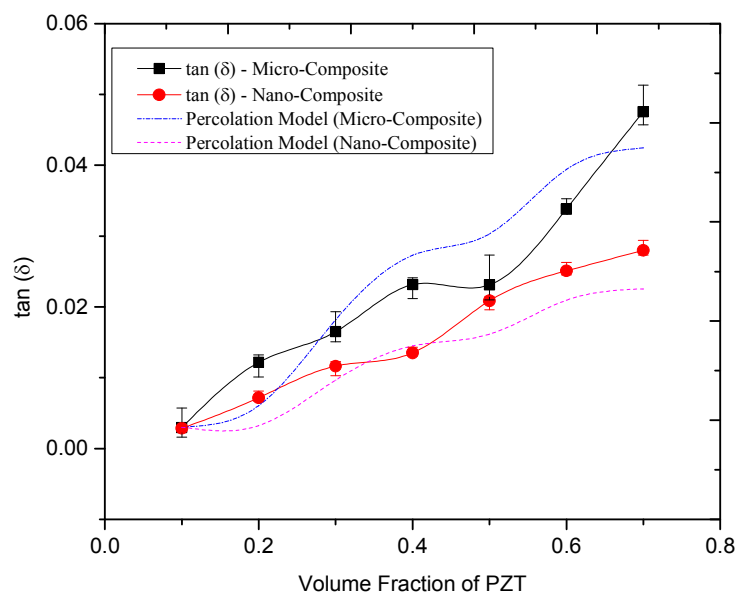


Figure 4-3 Comparison of the dielectric loss factor, $\tan \delta$ of the three phase composite with micro and nano sized Al inclusions and with the power law for the loss tangent

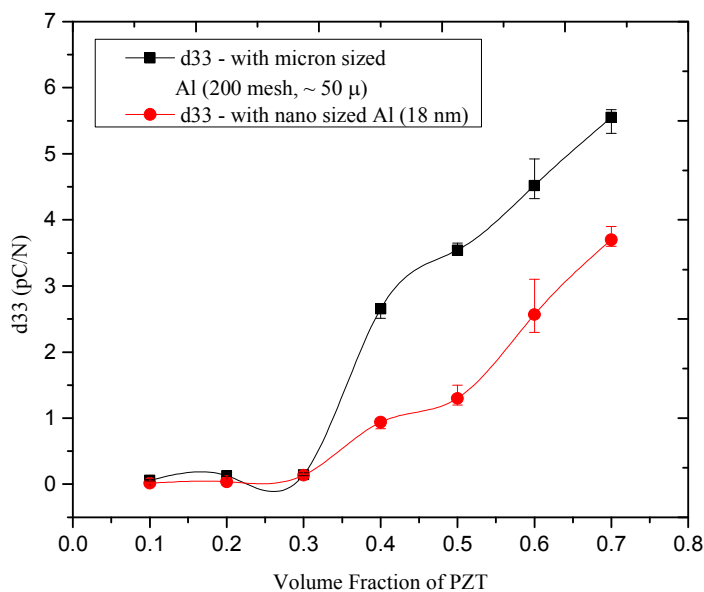


Figure 4-4 Comparison of the piezoelectric strain coefficient, d_{33} for the three phase micro and nano composite shows that the d_{33} values for both the set of composites increase after the volume fraction of PZT increases above 30% and that the values of the nano composite are lower than that of the micro composite

In Figures 4-5 and 4-6, SEM micrographs of three phase PZT– Epoxy–Al nano-composites at magnifications of 50,000 X and 100,000 X are presented respectively. These images show the distribution and clusters of the Al nano-particles in the epoxy matrix where the PZT volume fraction is 50% and Al volume fraction at 20%. Clustering and agglomeration of the Aluminum nanoparticles are observed in these images. The difference in performance of the composites comprised of nano and micron size aluminum particles could be the result of several factors.

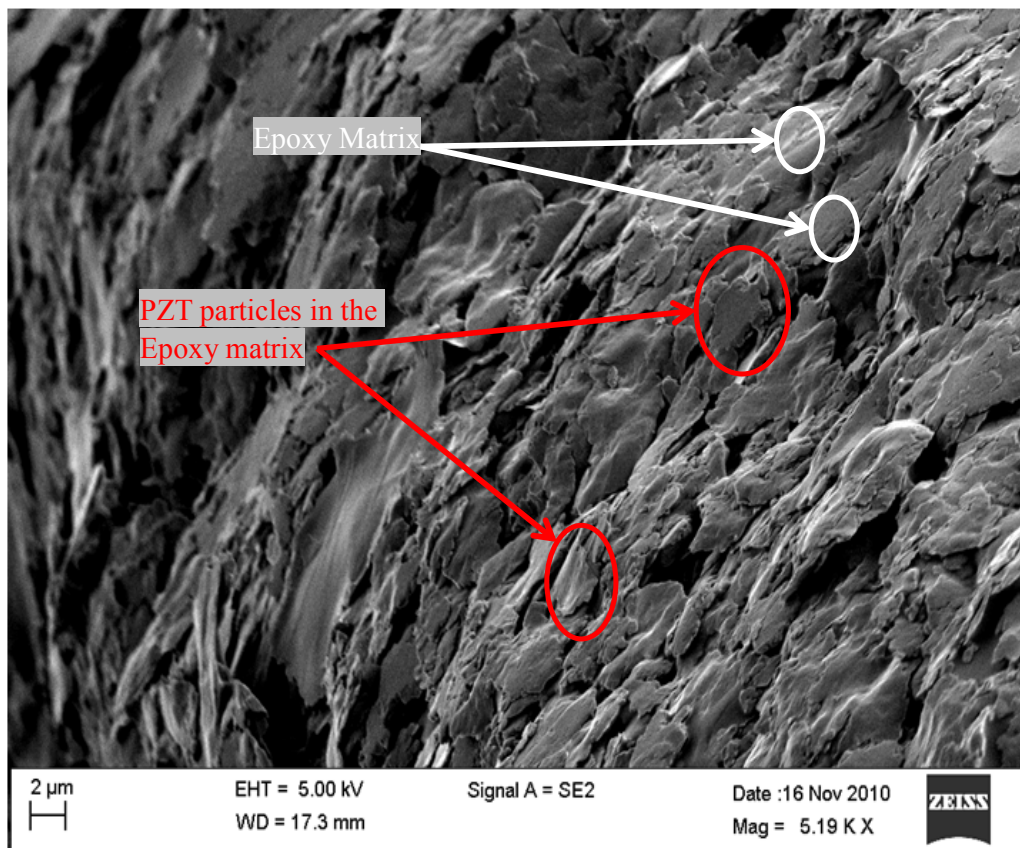


Figure 4-5 SEM micrograph of a three phase PZT-Epoxy-Al nano composite showing the distribution of the PZT particles in the Epoxy matrix with PZT volume

fraction at 50 % and Al volume fraction at 20 %

Contact resistance between the conductive material and the polymer matrix and dielectric material reduce the conductivity of the composite materials themselves. Das et al. [119] found that increasing the number density of particles in a composite increases the probability of particle to particle contact. Hence, nano-sized particles, which have a higher number density than micron sized particles, have a higher probability of surface contact with surrounding phases.

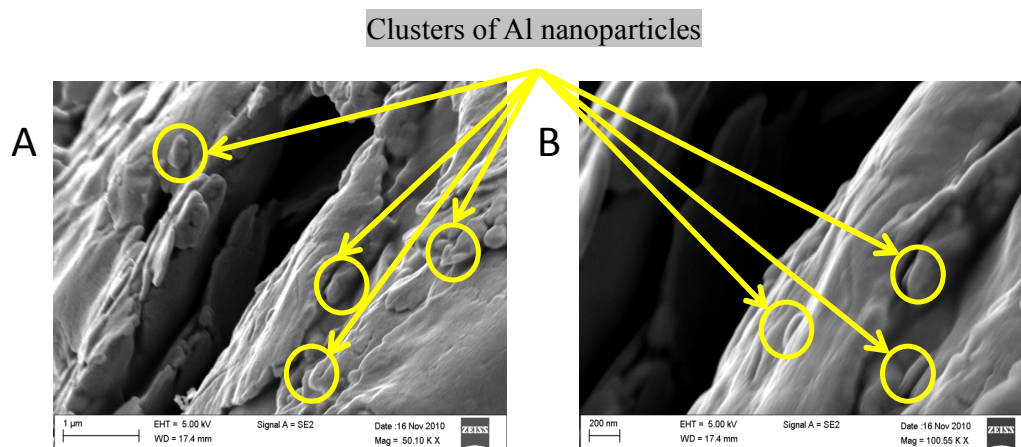


Figure 4-6 SEM micrographs of three phase PZT-Epoxy-Al nano composites at magnifications of A) 50,000 X and B) 100,000 X respectively showing the distribution and clusters of the Al nano particles in the Epoxy matrix with PZT volume fraction at 50 % and Al volume fraction at 20 %

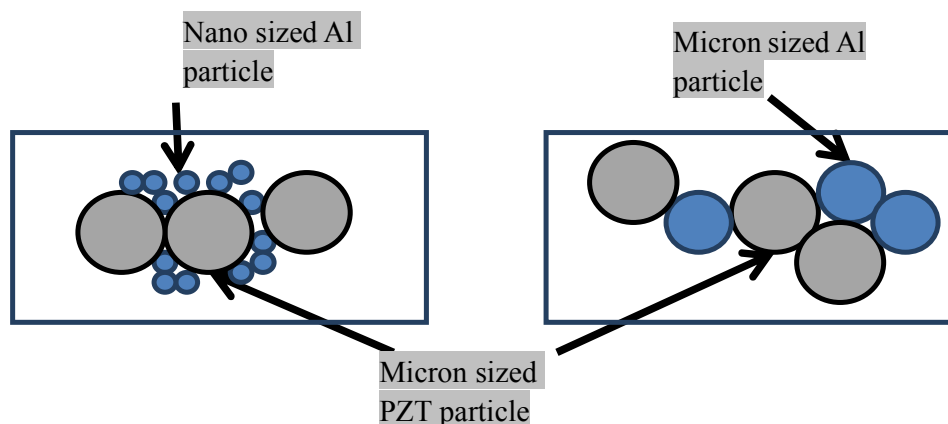


Figure 4-7 Contact points between Al a) nano sized and b) micron sized particles with the surrounding phases and with itself

This phenomenon is depicted in Figure 4-7. For example, Lee et al. [121] reported that the addition of nano-sized silver colloids to micro-sized silver flakes in a composite increased the resistivity. They concluded that the increase in resistivity was the result of increased contact resistance between the nano and micron sized particles. Novak et al. and Tchoudakov et al. [122, 124] suggested that networks were inhibited for forming in a three phase composite comprised of silver, epoxy and CB due to the mutual disturbance of the conductive networks, which they hypothesized to be due to the buildup of electrical charges on filler particle surfaces during mixing. In our work, the nano-sized Al particles have a higher number density of particles than micron sized particles within a composite. Thus, in some cases, there are more opportunities for contact of these materials with surrounding phases. As the size of the conductive inclusion diminishes, the probability of the number of contact points increases, which can lead to more contact resistance [39, 119, 121]. In Fig. 4-8, the bulk resistivity as a function of PZT volume fraction is portrayed for both sets of samples comprised of nano and micron sized aluminum particles. This figure shows that beyond a PZT volume fraction of 0.3, the bulk resistance of the nano-composite is higher than that of the micro-composite which explains the deviation of d_{33} of the micro and nano-composites for PZT volume fractions >0.3 . These results are consistent with those found by Choi et al. [39]. Also, Zheng et al. [89] and Chen et al. [123] found that ferroelectric 0–3 composites exhibit enhanced permittivity and piezoelectric coefficients when the electrical conductivity of the matrix material was

increased. Hence, in cases where the electrical conductivity of the matrix is reduced, the overall piezoelectric coefficients should consequently diminish.

Also, composite homogeneity is a critical parameter in achieving optimal performance, and is a challenge to achieve due to space charge effects. Adequate dispersion of PZT and conductive filler within the polymer matrix, and minimal air voids are desirable. However, agglomeration of PZT and conductive filler material within the matrix is common [67], and can lead to reduced mechanical, electrical and conductive properties in the materials. Also, Karttunen [85] found that when silver nano-sized silver particles embedded within a thermoplastic elastomer were slightly agglomerated, the percolation threshold was 13–16%, and the resistance was $2.0 \times 10^{-1} \Omega\text{cm}$.

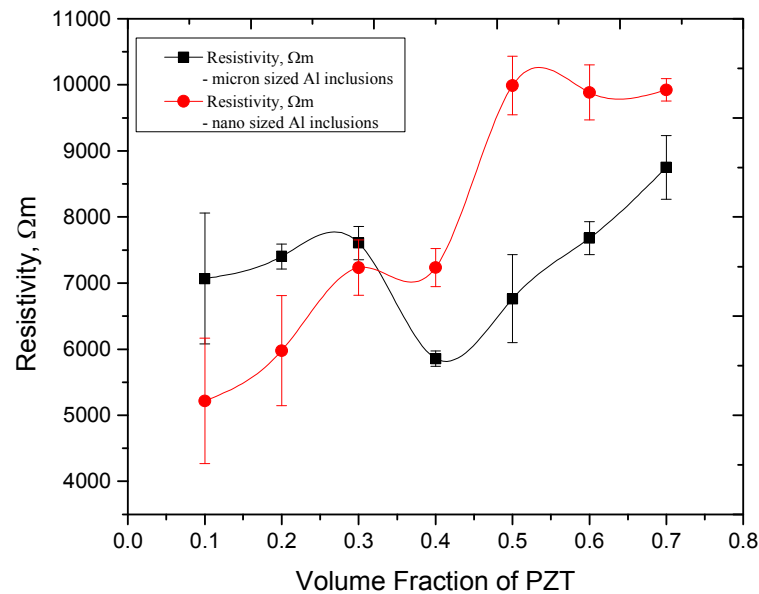


Figure 4-8 Resistivity of three phase micro and nano PZT-Epoxy-Al composites with varying PZT volume fraction

However, for heavily agglomerated particles, the percolation was 20% with higher

resistivity equal to $2.9 \times 10^3 \Omega \text{ cm}$. These results are similar in trend to those reported here in this study (Figure 4-8). Agglomeration was observed in the fabrication of both sets of composite materials, in particular those containing nano-size aluminum constituents. Also, the shapes of the micron sized aluminum inclusions are not perfectly spherical (as seen in Fig. 3-2 A), so as the aspect ratio of the inclusion increases, percolation threshold values can decrease, as opposed to particles that are more spherical in shape. The nano-sized particles in this study were more spherical in size in comparison to the micron sized inclusions. The addition of ceramic materials also tends to introduce flaws, in the form of agglomerations that contribute to scattering of results [67]. In order to achieve reduced void volume and agglomerations of material, enhanced fabrication techniques and additional studies are needed, which will be the subject in part of our future work.

4.3 Conclusions

Three phase epoxy/piezoelectric/conductive filler composites were fabricated. The volume fraction of the conductive filler, aluminum, was held constant at 20%, while the volume fraction of the piezoelectric material, PZT was varied from 0.10 to 0.70. Three sets of composites were examined, wherein, the size of the aluminum constituent was varied from micron in size (200 mesh) to nano in size ($\sim 18 \text{ nm}$). Both sets of composites presented enhanced loss factor ($\tan \delta$) and piezoelectric coefficient (d_{33}) values for volume fractions of PZT above 0.30. Composites having micron size aluminum particles exhibited higher loss factor, strain coefficients and dielectric constant than those that incorporated nano-size aluminum particles, which could be due to several factors:

agglomeration, contact resistance between particles, and excess air voids in the samples.

Chapter 5.

Conclusions and Future Work

5.1 Conclusions

In our present work analytical expressions for the estimation of the dielectric constant of three phase 0-3-0, piezoelectric-matrix-(conductive inclusion) composites, with spherical and spheroidal conductive inclusions has been developed based on the Maxwell-Garnett's approximation, and the Poon and Shin's model [64, 74, 108, 109]. This analytical model or the three phase model is validated by experimental results from Nan et al. [58] and Yao et al. [78]. Fabrication of piezoelectric composites with varying PZT volume fractions from 1% to 70% has shown that the piezoelectric and dielectric characteristics of the composites are enhanced by the increase of the PZT volume fraction due to the increase in the effective dipole moment of the piezoelectric component. The effective dielectric constant values of the two phase composite are overestimated by the Bruggeman's model and underestimated by the Maxwell Garnett's approximation due to the formation of the continuous agglomeration and the percolation clusters by the PZT particles which is validated by SEM micrographs.

Experimental results also indicate that addition of Aluminum, as a conductive inclusion (volume fraction is kept constant at 20%) also enhances the effective electromechanical properties of the composite. This is due to the increase in polarization of the effective electric field in the composite by the Aluminum particles which follows the power law for the effective dielectric constant of the composite in the percolation region. A study of the

increase in the volume fraction of Aluminum from 1% to 20% shows that the electromechanical properties are also enhanced by increasing Aluminum volume fraction before the composite reaches the percolation threshold. These results indicate that the percolation threshold can also be controlled by varying the PZT volume fraction in the three phase composite. The percolation threshold for the PZT-Epoxy-Al three phase composite is found to be about 17%. The variation in the dielectric and piezoelectric characteristics and the change in the percolation threshold with varying Aluminum and PZT volume fractions suggest that the smearing region of the percolation threshold can be tailored according to specific applications. Comparison of the three phase model indicates that the model is valid below the percolation limit and that the effect of percolation and the conductive inclusion size is not considered in the analytical model. The dielectric and piezoelectric properties of the composite also vary with the Aluminum inclusion size. Experimental results show that, with the variation of the Aluminum inclusion size from 200 mesh to ~18 nm, the micro composite show higher loss factor, strain coefficients and dielectric constant than those that in the nano-composite. This can be attributed to several factors which include the contact resistance between the particles in the microstructure, agglomeration and clustering of Aluminum and PZT particles and presence of air voids within the microstructure. The ease of processing, flexibility, and good dielectric behavior of the three-phase piezoelectric particulate composites potentially makes the composites suitable for practical applications in energy harvesting, acoustic dampening, embedded systems and structural health monitoring applications.

5.2 Future Work

The future work will include the incorporation of the effect of percolation and the effect of the conductive inclusion particle size in the three phase model for prediction of the effective dielectric constant for the three phase composite. The effect of the varying PZT volume fraction on the percolation threshold should be further investigated by fabrication and analysis of three phase composites by further variation of the PZT volume fraction. The effect of Multiwalled Carbon Nanotubes as spheroidal inclusions on the electromechanical properties of the three phase composite should also be experimentally investigated. A more precise understanding of the tailoring of the electromechanical properties by controlling the percolation threshold and the smearing region should be incorporated for both spherical and spheroidal inclusions. Thick film composite materials will be fabricated to understand both the d_{33} and d_{31} piezoelectric strain characteristics of these composite materials.

References

1. S. R. Anton and H. A. Sodano, "A review of power harvesting using piezoelectric materials (2003–2006)," *Smart Materials and Structures*, vol. 16, p. R1, 2007.
2. J. Baker, S. Roundy, and P. K. Wright, "Alternative Geometries for Increasing Power Density in Vibration Energy Scavenging for Wireless Sensor Networks," in *3rd International Energy Conversion Engineering Conference*, San Francisco, California, 2005.
3. H. Gu, Y. Zhao, and M. L. Wang, "A wireless smart PVDF sensor for structural health monitoring," *Structural Control and Health Monitoring*, vol. 12, pp. 329-343, 2005.
4. Y. Qi, N. T. Jafferis, K. Lyons, C. M. Lee, H. Ahmad, and M. C. McAlpine, "Piezoelectric Ribbons Printed onto Rubber for Flexible Energy Conversion," *Nano Letters*, vol. 10, pp. 524-528, 2010/02/10 2010.
5. S. J. Roundy, "Energy Scavenging for Wireless Sensor Nodes with a Focus on Vibration to Electricity Conversion," Doctor of Philosophy, Mechanical Engineering, The University of California, Berkeley, 2003.
6. S. Roundy, P. K. Wright, and J. M. Rabaey, *Energy Scavenging for Wireless Sensor Networks: With Special Focus on Vibrations*: Kluwer Academic Publishers, 2004.
7. Z. Shen, W. Y. Shih, and W.-H. Shih, "Mass detection sensitivity of piezoelectric cantilevers with a nonpiezoelectric extension," *Review of Scientific Instruments*, vol. 77, p. 065101, 2006.
8. Y. Man-Soon, H. Sung-Moo, and U. Soon-Chul, "A newly designed chopper for pyroelectric infrared sensor by using a dome-shaped piezoelectric linear motor (DSPLM)," *Journal of Electroceramics*, vol. 23, pp. 242-247, 2009/10/01 2009.
9. L. P. Wang, K. Deng, L. Zou, R. Wolf, R. J. Davis, and S. Trolier-McKinstry, "Microelectromechanical systems (MEMS) accelerometers using lead zirconate titanate thick films," *Electron Device Letters, IEEE*, vol. 23, pp. 182-184, 2002.
10. W. Li-Peng, R. A. Wolf, Jr., W. Yu, K. K. Deng, L. Zou, R. J. Davis, and S. Trolier-McKinstry, "Design, fabrication, and measurement of high-sensitivity piezoelectric microelectromechanical systems accelerometers," *Microelectromechanical Systems, Journal of*, vol. 12, pp. 433-439, 2003.
11. C. H. Cheng and S. L. Tu, "Fabrication of a novel piezoelectric actuator with high load-bearing capability," *Sensors and Actuators A: Physical*, vol. 141, pp. 160-165, 2008.
12. C. Jongpil, G. Abhijat, A. T. Srinivas, and D. R. Christopher, "Fabrication and performance of a flextensional microactuator," *Journal of Micromechanics and Microengineering*, vol. 15, p. 1947, 2005.

13. O. Delas, A. Berry, P. Masson, and Y. Pasco, "Optimizing the thickness of piezoceramic actuators for bending vibration of planar structures," *Journal of Intelligent Material Systems and Structures*, vol. 18, pp. 1191-1201, 2007.
14. S.-C. Woo, K. H. Park, and N. S. Goo, "Influences of dome height and stored elastic energy on the actuating performance of a plate-type piezoelectric composite actuator," *Sensors and Actuators A: Physical*, vol. 137, pp. 110-119, 2007.
15. R. G. Polcawich and T. P. S. University, *Design, Fabrication, Test, and Evaluation of RF MEMS Series Switches Using Lead Zirconate Titanate (PZT) Thin Film Actuators*: The Pennsylvania State University, 2007.
16. K. S. S. Ram and S. K. Kiran, "Static behaviour of a laminated composite spherical shell cap with piezoelectric actuators," *Smart Materials and Structures*, vol. 17, p. 035010, 2008.
17. H. Chandralalim, S. A. Bhave, R. Polcawich, J. Pulskamp, D. Judy, R. Kaul, and M. Dubey, "Performance comparison of $\text{Pb}(\text{Zr}_{0.52}\text{Ti}_{0.48})\text{O}_3$ -only and $\text{Pb}(\text{Zr}_{0.52}\text{Ti}_{0.48})\text{O}_3$ -on-silicon resonators," *Applied Physics Letters*, vol. 93, pp. 233504-3, 2008.
18. B. P. Otis and J. M. Rabaey, "A 300-micro W 1.9-GHz CMOS oscillator utilizing micromachined resonators," *Solid-State Circuits, IEEE Journal of*, vol. 38, pp. 1271-1274, 2003.
19. S. V. Krishnaswamy, J. Rosenbaum, S. Horwitz, C. Yale, and R. A. Moore, "Compact FBAR filters offer low-loss performance," *Microwaves & RF*, pp. 127-136, 1991.
20. K. M. Lakin, G. R. Kline, and K. T. McCarron, "High Q microwave acoustic resonators and filters," in *Microwave Symposium Digest, 1993., IEEE MTT-S International*, 1993, pp. 1517-1520 vol.3.
21. X. Jiang, K. Snook, T. Walker, A. Portune, R. Haber, X. Geng, J. Welter, and W. S. Hackenberger, "Single crystal piezoelectric composite transducers for ultrasound NDE applications," pp. 69340D-69340D, 2008.
22. F. Guo-Hua, "A piezoelectric dome-shaped-diaphragm transducer for microgenerator applications," *Smart Materials and Structures*, vol. 16, p. 2636, 2007.
23. F. Guo-Hua Feng Guo-Hua and K. Eun Sok Kim Eun Sok, "Piezoelectrically actuated dome-shaped diaphragm micropump," *J Microelectromech Syst*, vol. 14, pp. 192-199, 2005.
24. F. Guo-Hua, C. C. Sharp, Z. Qifa, P. Wei, K. Eun Sok, and K. K. Shung, "Fabrication of MEMS ZnO dome-shaped-diaphragm transducers for high frequency ultrasonic imaging [biomedical imaging]," in *Ultrasonics Symposium, 2004 IEEE*, 2004, pp. 1950-1953 Vol.3.

25. A. Fleischman, R. Modi, A. Nair, J. Talman, G. Lockwood, and S. Roy, "Miniature high frequency focused ultrasonic transducers for minimally invasive imaging procedures," *Sensors and Actuators A: Physical*, vol. 103, pp. 76-82, 2003.
26. K. Liang, H. Kunkel, C. Oakley, and W. Huebner, "Acoustic characterization of ultrasonic transducer materials: I. Blends of rigid and flexible epoxy resins used in piezocomposites," *Ultrasonics*, vol. 36, pp. 979-986, 1998.
27. K. Liang, C. Oakley, W. Huebner, and H. Kunkel, "Acoustic characterization of ultrasonic transducer materials: II. The effect of curing agent in binary epoxy blends on acoustic properties," *Ultrasonics*, vol. 37, pp. 201-207, 1999.
28. J. Peng, C. Chao, and H. Tang, "Piezoelectric micromachined ultrasonic transducer based on dome-shaped piezoelectric single layer," *Microsystem Technologies*, vol. 16, pp. 1771-1775, 2010/10/01 2010.
29. D. P. Skinner, R. E. Newnham, and L. E. Cross, "Flexible composite transducers," *Materials Research Bulletin*, vol. 13, pp. 599-607, 1978.
30. O. B. Wilson, U. S. N. S. S. Command, and U. S. N. E. S. Command, *An introduction to the theory and design of sonar transducers*: Naval Sea Systems Command, 1985.
31. Q. Q. Zhang, F. T. Djuth, Q. F. Zhou, C. H. Hu, J. H. Cha, and K. K. Shung, "High frequency broadband PZT thick film ultrasonic transducers for medical imaging applications," *Ultrasonics*, vol. 44, Supplement, pp. e711-e715, 2006.
32. Y. Bai, Z. Y. Cheng, V. Bharti, H. S. Xu, and Q. M. Zhang, "High-dielectric-constant ceramic-powder polymer composites," *Applied Physics Letters*, vol. 76, pp. 3804-3806, 2000.
33. D.-H. Kuo, C.-C. Chang, T.-Y. Su, W.-K. Wang, and B.-Y. Lin, "Dielectric behaviours of multi-doped BaTiO₃/epoxy composites," *Journal of the European Ceramic Society*, vol. 21, pp. 1171-1177, 2001.
34. R. Funer, "Embedding Resistors and Capacitors," *Printed Circuit Des.*, vol. 19, p. 8, 2002.
35. R. Ulrich, "Matching Embedded Capacitor Dielectrics to Applications," *Circuit World*, vol. 30, p. 20, 2004.
36. S. Bhattacharya and R. Tummala, "Next generation integral passives: materials, processes, and integration of resistors and capacitors on PWB substrates," *Journal of Materials Science: Materials in Electronics*, vol. 11, pp. 253-268, 2000/04/01 2000.
37. S. K. Bhattacharya and R. R. Tummala, "Epoxy Nanocomposite Capacitors for Application as MCM-L Compatible Integral Passives," *Journal of Electronic Packaging*, vol. 124, pp. 1-6, 2002.
38. H.-W. Choi, Y.-W. Heo, J.-H. Lee, J.-J. Kim, H.-Y. Lee, E.-T. Park, and Y.-K. Chung, "Effects of BaTiO₃ on dielectric behavior of BaTiO₃--Ni--polymethyl methacrylate composites," *Applied Physics Letters*, vol. 89, pp. 132910-3, 2006.

39. H.-W. Choi, Y.-W. Heo, J.-H. Lee, J.-J. Kim, H.-Y. Lee, E.-T. Park, and Y.-K. Chung, "Effects of Ni Particle Size on Dielectric Properties of PMMA-Ni-BaTiO₃ Composites," *Integrated Ferroelectrics*, vol. 87, pp. 85-93, 2007.
40. K. Hyungsoo, S. Byung Kook, and K. Joungho, "Suppression of GHz range power/ground inductive impedance and simultaneous switching noise using embedded film capacitors in multilayer packages and PCBs," *Microwave and Wireless Components Letters, IEEE*, vol. 14, pp. 71-73, 2004.
41. L. Li, A. Takahashi, J. J. Hao, R. Kikuchi, T. Hayakawa, T. A. Tsurumi, and M. A. Kakimoto, "Novel Polymer-Ceramic Nanocomposite Based on New Concepts for Embedded Capacitor Application (I)," in *IEEE Trans. Compon. Packag. Technol.*, 2005, p. 754.
42. S. Ogitan, S. A. Bidstrup-Allen, and P. A. Kohl, "Factors influencing the permittivity of polymer/ceramic composites for embedded capacitors," *Advanced Packaging, IEEE Transactions on*, vol. 23, pp. 313-322, 2000.
43. Y. Rao and C. P. Wong, "Material characterization of a high-dielectric-constant polymer-ceramic composite for embedded capacitor for RF applications," *Journal of Applied Polymer Science*, vol. 92, pp. 2228-2231, 2004.
44. Z. Li, D. Zhang, and K. Wu, "Cement-Based 0-3 Piezoelectric Composites," *Journal of the American Ceramic Society*, vol. 85, pp. 305-313, 2002.
45. B. Dong and Z. Li, "Cement-based piezoelectric ceramic smart composites," *Composites Science and Technology*, vol. 65, pp. 1363-1371, 2005.
46. S. Huang, J. Chang, L. Lu, F. Liu, Z. Ye, and X. Cheng, "Preparation and polarization of 0-3 cement based piezoelectric composites," *Materials Research Bulletin*, vol. 41, pp. 291-297, 2006.
47. P. Blanas and D. K. Das-Gupta, "Composite Piezoelectric Materials for Health Monitoring of Composite Structures," in *Material Research Society Symposium*, 2000.
48. S. Shao, J. Zhang, Z. Zhang, P. Zheng, M. Zhao, J. Li, and C. Wang, "High piezoelectric properties and domain configuration in BaTiO₃ ceramics obtained through solid-state reaction route," *Journal of Physics D: Applied Physics*, vol. 42, p. 189801, 2009.
49. S. Wada, K. Yako, H. Kakimoto, T. Tsurumi, and T. Kiguchi, "Enhanced piezoelectric properties of barium titanate single crystals with different engineered-domain sizes," *Journal of Applied Physics*, vol. 98, pp. 014109-7, 2005.
50. S. Wada, K. Yamato, P. Pulpan, N. Kumada, B.-Y. Lee, T. Iijima, C. Moriyoshi, and Y. Kuroiwa, "Piezoelectric properties of high Curie temperature barium titanate-bismuth perovskite-type oxide system ceramics," *Journal of Applied Physics*, vol. 108, pp. 094114-5, 2010.

51. Y. Xiang, R. Zhang, and W. Cao, "Piezoelectric properties of domain engineered barium titanate single crystals with different volume fractions of domain walls," *Journal of Applied Physics*, vol. 106, pp. 064102-5, 2009.
52. H.-D. Nam and H. Y. Lee, "Fabrication and Piezoelectric Properties of PZT Ceramics Prepared by Partial Oxalate Method," presented at the Proceedings of the Eighth IEEE International Symposium 1992.
53. Y. Takahiro, K. Masako, and S. Norikazu, "Influence of poling conditions on the piezoelectric properties of PZT ceramics," *Journal of Materials Science: Materials in Electronics*, vol. 11, pp. 425-428, 2000.
54. W. Da-Wei, J. Hai-Bo, Y. Jie, W. Bao-Li, Z. Quan-Liang, Z. De-Qing, and C. Mao-Sheng, "Mechanical Reinforcement and Piezoelectric Properties of PZT Ceramics Embedded with Nano-Crystalline," *Chinese Physics Letters*, vol. 27, p. 047701, 2010.
55. K. L. Yadav and R. N. P. Choudhary, "Piezoelectric Properties of Modified PZT Ceramics," *Ferroelectrics*, vol. 325, pp. 87-94, 2005.
56. R. E. Newnham, D. P. Skinner, K. A. Klicker, A. S. Bhalla, B. Hardimana, and T. R. Gururajaa, "Ferroelectric ceramic-plastic composites for piezoelectric and pyroelectric applications," *Ferroelectrics*, vol. 27, pp. 49-55, 1980.
57. S. M. Pilgrim and R. E. Newnham, "3:0: A new composite connectivity," *Materials Research Bulletin*, vol. 21, pp. 1447-1454, 1986.
58. M. I. Bichurin and G. Srinivasan, "Magnetoelectric effect in porous bulk ferromagnetic/piezoelectric composites," in *APS March Meeting*, 2005.
59. C. W. Nan, L. Liu, N. Cai, J. Zhai, Y. Ye, Y. H. Lin, L. J. Dong, and C. X. Xiong, "A three-phase magnetoelectric composite of piezoelectric ceramics, rare-earth iron alloys, and polymer," *Applied Physics Letters*, vol. 81, pp. 3831-3833, 2002.
60. V. Y. Topolov, B. P., and C. R. Bowen, "Analysis of the piezoelectric performance of modern 0-3-type composites based on relaxor-ferroelectric single crystals," *Ferroelectrics*, vol. 413, pp. 176-191, 2011.
61. L. F. Cai, Y. L. Mai, M. Z. Rong, and W. H. Ruan, "Interfacial Effects in Nano-Silica/Polypropylene Composites Fabricated by In-Situ Chemical Blowing," *eXPRESS Polymer Letters*, vol. 1, pp. 2-7, 2007.
62. C. W. Nan, M. Li, and J. H. Huang, "Calculations of giant magnetoelectric effects in ferroic composites of rare-earth-iron alloys and ferroelectric polymers," *Physical Review B*, vol. 63, p. 144415, 2001.
63. L. Qi, B. I. Lee, W. D. Samuels, G. J. Exarhos, and S. G. Parler, "Three-phase percolative silver-BaTiO₃-epoxy nanocomposites with high dielectric constants," *Journal of Applied Polymer Science*, vol. 102, pp. 967-971, 2006.

64. C. H. Ho, Y. M. Poon, and F. G. Shin, "New explicit formulas for the effective piezoelectric coefficients of binary 0-3 composites," *Journal of Electroceramics*, vol. 16, pp. 283-288, 2006.
65. M. Ma and X. Wang, "Preparation, microstructure and properties of epoxy-based composites containing carbon nanotubes and PMN-PZT piezoceramics as rigid piezo-damping materials," *Materials Chemistry and Physics*, vol. 116, pp. 191-197, 2009.
66. S. Tian and X. Wang, "Fabrication and performances of epoxy/multi-walled carbon nanotubes/piezoelectric ceramic composites as rigid piezo-damping materials," *Journal of Materials Science*, vol. 43, pp. 4979-4987, 2008.
67. S. Tsantzalis, P. Karapappas, A. Vavouliotis, P. Tsotra, A. Paipetis, V. Kostopoulos, and K. Friedrich, "Enhancement of the mechanical performance of an epoxy resin and fiber reinforced epoxy resin composites by the introduction of CNF and PZT particles at the microscale," *Composites Part A: Applied Science and Manufacturing*, vol. 38, pp. 1076-1081, 2007.
68. W. T. Doyle and I. S. Jacobs, "The influence of particle shape on dielectric enhancement in metal-insulator composites," *Journal of Applied Physics*, vol. 71, pp. 3926-3936, 1992.
69. E. H. Kerner, "The Electrical Conductivity of Composite Media," *Proceedings of the Physical Society. Section B*, vol. 69, p. 802, 1956.
70. D. A. G. Bruggeman, "Berechnung verschiedener physikalischer Konstanten von heterogenen Substanzen. I. Dielektrizitätskonstanten und Leitfähigkeiten der Mischkörper aus isotropen Substanzen," *Annalen der Physik*, vol. 416, pp. 636-664, 1935.
71. K. W. Wagner, "The Theory of Incomplete Dielectricity," *Ann. Phys.*, vol. 40, p. 817, 1913.
72. Y. M. Poon and F. G. Shin, "A simple explicit formula for the effective dielectric constant of binary 0-3 composites," *Journal of Materials Science*, vol. 39, pp. 1277-1281, 2004.
73. N. Jayasundere and B. V. Smith, "Dielectric constant for binary piezoelectric 0-3 composites," *Journal of Applied Physics*, vol. 73, pp. 2462-2466, 1993.
74. J. C. M. Garnett, "Colours in Metal Glasses, in Metallic Films, and in Metallic Solutions. II," *Phil. Trans. R. Soc. Lond.*, vol. 205, pp. 237-288, 1906.
75. C. W. Nan, *Physics of Inorganic Homogenous Materials*: Pergamon, Progress in Material Science 1993.
76. K. Han, A. Safari, and R. E. Riman, "Colloidal Processing for Improved Piezoelectric Properties of Flexible 0-3 Ceramic-Polymer Composites," *Journal of the American Ceramic Society*, vol. 74, pp. 1699-1702, 1991.

77. S.-H. Yao, Z.-M. Dang, M.-J. Jiang, and J. Bai, "BaTiO₃-carbon nanotube/polyvinylidene fluoride three-phase composites with high dielectric constant and low dielectric loss," *Applied Physics Letters*, vol. 93, pp. 182905-3, 2008.
78. M. Hori, T. Aoki, Y. Ohira, and S. Yano, "New type of mechanical damping composites composed of piezoelectric ceramics, carbon black and epoxy resin," *Composites Part A: Applied Science and Manufacturing*, vol. 32, pp. 287-290, 2001.
79. Z. M. Dang, Y. Shen, and C. W. Nan, "Dielectric behavior of three-phase percolative Ni-BaTiO₃/polyvinylidene fluoride composites," *Applied Physics Letters*, vol. 81, pp. 4814-4816, 2002.
80. S. G. Miller and T. U. o. Akron, *Effects of Nanoparticle and Matrix Interface on Nanocomposite Properties*: The University of Akron, 2008.
81. Z. Ma, M. G. Smith, S. K. Richards, and X. Zhang, "Attenuation of slat trailing edge noise using acoustic liners," *aeroacoustics*, vol. 5, pp. 311-333, 2006.
82. J. K. Nelson, *Dielectric Polymer Nanocomposites*: Springer, 2010.
83. "Dielectric Elastomers as Electromechanical Transducers: Fundamentals, Materials, Devices, Models and Applications of an Emerging Electroactive Polymer Technology," in *Dielectric Elastomers as Electromechanical Transducers*, C. Federico, R. Danilo De, K. Roy, P. Ronald, and S.-L. Peter, Eds., ed Amsterdam: Elsevier, 2008, pp. 321-329.
84. B. Li-Rong, W. Bin, and A. Y. Xiao, "Conductive Coating Formulations with Low Silver Content," in *Electronic Components and Technology Conference, 2007. ECTC '07. Proceedings. 57th*, 2007, pp. 494-500.
85. M. Karttunen, P. Ruuskanen, V. Pitkänen, and W. Albers, "Electrically Conductive Metal Polymer Nanocomposites for Electronics Applications," *Journal of Electronic Materials*, vol. 37, pp. 951-954, 2008/07/01 2008.
86. X. M. Chen, J. W. Shen, and W. Y. Huang, "Novel electrically conductive polypropylene/graphite nanocomposites," *Journal of Materials Science Letters*, vol. 21, pp. 213-214, 2002.
87. D.-L. Shi, X.-Q. Feng, Y. Y. Huang, K.-C. Hwang, and H. Gao, "The Effect of Nanotube Waviness and Agglomeration on the Elastic Property of Carbon Nanotube-Reinforced Composites," *Journal of Engineering Materials and Technology*, vol. 126, pp. 250-257, 2004.
88. W.-G. Weng, G.-H. Chen, D.-J. Wu, and W.-L. Yan, "HDPE/expanded graphite electrically conducting composite," *Composite Interfaces*, vol. 11, pp. 131-143, 2004.
89. W. Zheng and S.-C. Wong, "Electrical conductivity and dielectric properties of PMMA/expanded graphite composites," *Composites Science and Technology*, vol. 63, pp. 225-235, 2003.

90. L. Burianova, P. Hana, S. Panos, J. Kulek, and Y. I. Tyagur, "Piezoelectric, dielectric and pyroelectric properties of 0-3 ceramic-polymer composites," *Ferroelectrics*, vol. 241, pp. 59-66, 2000/03/01 2000.
91. K. L. Chan, M. Mariatti, Z. Lockman, and L. C. Sim, "Effects of the size and filler loading on the properties of copper- and silver-nanoparticle-filled epoxy composites," *Journal of Applied Polymer Science*, vol. 121, pp. 3145-3152, 2011.
92. N. Guo, S. A. DiBenedetto, P. Tewari, M. T. Lanagan, M. A. Ratner, and T. J. Marks, "Nanoparticle, Size, Shape, and Interfacial Effects on Leakage Current Density, Permittivity, and Breakdown Strength of Metal Oxide–Polyolefin Nanocomposites: Experiment and Theory," *Chemistry of Materials*, vol. 22, pp. 1567-1578, 2010.
93. R. Qiao, H. Deng, K. W. Putz, and L. C. Brinson, "Effect of particle agglomeration and interphase on the glass transition temperature of polymer nanocomposites," *Journal of Polymer Science Part B: Polymer Physics*, vol. 49, pp. 740-748, 2011.
94. G. Suriati, M. Mariatti, and A. Azizan, "Effects of filler shape and size on the properties of silver filled epoxy composite for electronic applications," *Journal of Materials Science: Materials in Electronics*, vol. 22, pp. 56-63, 2011.
95. S. A. Zavyalov, A. N. Pivkina, and J. Schoonman, "Formation and characterization of metal-polymer nanostructured composites," *Solid State Ionics*, vol. 147, pp. 415-419, 2002.
96. J. B. Bai and A. Allaoui, "Effect of the length and the aggregate size of MWNTs on the improvement efficiency of the mechanical and electrical properties of nanocomposites—experimental investigation," *Composites Part A: Applied Science and Manufacturing*, vol. 34, pp. 689-694, 2003.
97. W. Bauhofer and J. Z. Kovacs, "A review and analysis of electrical percolation in carbon nanotube polymer composites," *Composites Science and Technology*, vol. 69, pp. 1486-1498, 2009.
98. J. Chang, G. Liang, A. Gu, S. Cai, and L. Yuan, "The production of carbon nanotube/epoxy composites with a very high dielectric constant and low dielectric loss by microwave curing," *Carbon*, vol. 50, pp. 689-698, 2012.
99. F.-C. Chiu and G.-F. Kao, "Polyamide 46/multi-walled carbon nanotube nanocomposites with enhanced thermal, electrical, and mechanical properties," *Composites Part A: Applied Science and Manufacturing*, vol. 43, pp. 208-218, 2012.
100. S. M. Zhang, L. Lin, H. Deng, X. Gao, E. Bilotti, T. Peijs, Q. Zhang, and Q. Fu, "Synergistic effect in conductive networks constructed with carbon nanofillers in different dimensions," *eXPRESS Polymer Letters*, vol. 6, p. 159, 2012.
101. A. Shaulov and W. A. Smith, "Ultrasonic Transducer Arrays Made from Composite Piezoelectric Materials," in *IEEE 1985 Ultrasonics Symposium*, 1985, pp. 648-651.

102. E. Venkatragavaraj, B. Satish, P. R. Vinod, and M. S. Vijaya, "Piezoelectric properties of ferroelectric PZT-polymer composites," *Journal of Physics D: Applied Physics*, vol. 34, p. 487, 2001.
103. F. Levassort, M. Lethiecq, T. Gomez, F. Montero de Espinosa, A. James, E. Ringgard, P. Hawkins, and C. E. Millar, "Modeling the effective properties of highly loaded 0-3 piezocomposites," in *Ultrasonics Symposium, 1996. Proceedings., 1996 IEEE*, 1996, pp. 463-466 vol.1.
104. C. Huang, Q. M. Zhang, G. deBotton, and K. Bhattacharya, "All-organic dielectric-percolative three-component composite materials with high electromechanical response," *Applied Physics Letters*, vol. 84, pp. 4391-4393, 2004.
105. X. Yu and E. Kwon, "A carbon nanotube/cement composite with piezoresistive properties," *Smart Materials and Structures*, vol. 18, p. 055010, 2009.
106. Z. M. Dang, L. Z. Fan, Y. Shen, and C. W. Nan, "Dielectric behavior of novel three-phase MWNTs/BaTiO₃/PVDF composites," *Materials Science and Engineering: B*, vol. 103, pp. 140-144, 2003.
107. A. Voet, "Dielectrics and rheology of non-aqueous dispersions," *The Journal of physical and colloid chemistry*, vol. 51, pp. 1037-1063, 1947.
108. K. Lal and R. Parshad, "Permittivity of conductor-dielectric heterogeneous mixtures," *Journal of Physics D: Applied Physics*, vol. 6, p. 1788, 1973.
109. S. Banerjee and K. A. Cook-Chennault, "An Analytical Model for the Effective Dielectric Constant of a 0-3-0 Composite," *Journal of Engineering Materials and Technology*, vol. 133, pp. 041005-5, 2011.
110. S. Banerjee and K. A. Cook-Chennault, "Influence of Al Particle Size and Lead Zirconate Titanate (PZT) Volume Fraction on the Dielectric Properties of PZT-Epoxy-Aluminum Composites," *Journal of Engineering Materials and Technology*, vol. 133, pp. 041016-6, 2011.
111. C. T. O'Konski, "Electric Properties of Macromolecules. V. Theory of Ionic Polarization in Polyelectrolytes," *Physica*, vol. 12, p. 257, 1960.
112. K. A. Cook-Chennault, N. Thambi, M. A. Bitetto, and E. B. Hameyie, "Piezoelectric Energy Harvesting: A Green and Clean Alternative for Sustained Power Production," *Bull Sci Technol Soc*, vol. 28, pp. 496-509, 2008.
113. G. Gautschi, *Piezoelectric Sensorics: Force, Strain, Pressure, Acceleration and Acoustic Emission Sensors, Materials and Amplifiers*: Springer, 2006.
114. T. Zhang, M. Zhao, and P. Tong, "Fracture of piezoelectric ceramics," *Advances in Applied Mechanics*, pp. 147-289, 2001.
115. W. Shields, J. Ro, and A. Baz, "Control of sound radiation from a plate into an acoustic cavity using active piezoelectric-damping composites," *Smart Materials and Structures*, vol. 7, p. 1, 1998.

116. S. Banerjee and K. A. Cook-Chennault, "An investigation into the influence of electrically conductive particle size on electromechanical coupling and effective dielectric strain coefficients in three phase composite piezoelectric polymers," *Composites Part A: Applied Science and Manufacturing*, vol. 43, pp. 1612-1619, 2012.
117. L. Qi, B. I. Lee, S. Chen, W. D. Samuels, and G. J. Exarhos, "High-Dielectric-Constant Silver-Epoxy Composites as Embedded Dielectrics," *Advanced Materials*, vol. 17, pp. 1777-1781, 2005.
118. Z. Ahmad, A. Prasad, and K. Prasad, "A comparative approach to predicting effective dielectric, piezoelectric and elastic properties of PZT/PVDF composites," *Physica B: Condensed Matter*, vol. 404, pp. 3637-3644, 2009.
119. R. N. Das, F. D. Egitto, and V. R. Markovich, "Nano- and micro-filled conducting adhesives for z-axis interconnections: new direction for high-speed, high-density, organic microelectronics packaging," *Circuit World*, vol. 34, pp. 3-12, 2008.
120. C. A. Martin, J. K. W. Sandler, M. S. P. Shaffer, M. K. Schwarz, W. Bauhofer, K. Schulte, and A. H. Windle, "Formation of percolating networks in multi-wall carbon-nanotube-epoxy composites," *Composites Science and Technology*, vol. 64, pp. 2309-2316, 2004.
121. H.-H. Lee, K.-S. Chou, and Z.-W. Shih, "Effect of nano-sized silver particles on the resistivity of polymeric conductive adhesives," *International Journal of Adhesion and Adhesives*, vol. 25, pp. 437-441, 2005.
122. I. Novák, I. Krupa, and I. Chodák, "Analysis of correlation between percolation concentration and elongation at break in filled electroconductive epoxy-based adhesives," *European Polymer Journal*, vol. 39, pp. 585-592, 2003.
123. G.-H. Chen, D.-J. Wu, W.-G. Weng, and W.-L. Yan, "Preparation of polymer/graphite conducting nanocomposite by intercalation polymerization," *Journal of Applied Polymer Science*, vol. 82, pp. 2506-2513, 2001.
124. R. Tchoudakov, O. Breuer, M. Narkis, and A. Siegmann, "Conductive polymer blends with low carbon black loading: Polypropylene/polyamide," *Polymer Engineering & Science*, vol. 36, pp. 1336-1346, 1996.
125. S. Banerjee and K. A. Cook-Chennault, "Influence of Al inclusions and PZT volume fraction on the dielectric and piezoelectric characteristics of three phase PZT-Cement-Al composites," *Current Cement Research*, Accepted.
126. S. Banerjee, W. L. Du, L. Wang, and K. A. Cook-Chennault, "Fabrication of Dome-Shaped PZT-Epoxy Actuator Using Sol-Gel and Spin Coating Technique," *Journal of Electroceramics*, In Press.